

# Extension and optimization of the FIND algorithm: computing Green's and less-than Green's functions (with technical appendix)

S. Li<sup>a</sup>, E. Darve<sup>a,b</sup>

<sup>a</sup>Institute for Computational and Mathematical Engineering, Stanford University,  
496 Lomita Mall, Durand building, Stanford, CA 94305, USA,

<sup>b</sup>Department of Mechanical Engineering, Stanford University,  
496 Lomita Mall, Durand Building, Room 209, Stanford, CA 94305, USA,  
darve@stanford.edu

May 9, 2019

**Abstract.** The FIND algorithm is a fast algorithm designed to calculate certain entries of the inverse of a sparse matrix. Such calculation is critical in many applications, e.g., quantum transport in nano-devices. We extended the algorithm to other matrix inverse related calculations. Those are required for example to calculate the less-than Green's function and the current density through the device. For a 2D device discretized as an  $N_x \times N_y$  mesh, the best known algorithms have a running time of  $\mathcal{O}(N_x^3 N_y)$ , whereas FIND only requires  $\mathcal{O}(N_x^2 N_y)$ . Even though this complexity has been reduced by an order of magnitude, the matrix inverse calculation is still the most time consuming part in the simulation of transport problems. We could not reduce the order of complexity, but we were able to significantly reduce the constant factor involved in the computation cost. By exploiting the sparsity and symmetry, the size of the problem beyond which FIND is faster than other methods typically decreases from a  $130 \times 130$  2D mesh down to a  $40 \times 40$  mesh. These improvements make the optimized FIND algorithm even more competitive for real-life applications.

## Main Notations

---

$M$	the set of all the nodes in the mesh, p. 5
$T$	the mesh is subdivided using nested dissection; $T$ is the resulting tree of clusters, p. 5
$C, C_g$	$C$ is a set of mesh nodes after the partitioning. It is sometimes called a cluster. It may designate a cluster at any level in the tree. A specific cluster is denoted as $C_g$ , where $g$ is the label used when partitioning the whole mesh, as shown in Fig. 1(a).
$\bar{C}, C_{-g}$	$\bar{C}$ is the complement of $C$ with respect to $M$ and $C_{-g} = \bar{C}_g$ as shown in Fig. 1(b). p. 5
$B, B_g$	set of boundary nodes of a cluster, $B_g$ is the set boundary nodes of $C_g$ and sometimes called the boundary set of $C_g$ . p. 7
$B_L, B_R$	sets of boundary nodes originated from the left child cluster and the right cluster, p. 13
$I, I_g$	set of inner nodes. $I_g$ is the set of inner nodes of $C_g$ . $I_g \cap B_g = \emptyset$ and $I_g \cup B_g = C_g$ . p. 7
$S, S_g$	set of private inner nodes. $S_g$ is the set of private inner nodes of cluster $C_g$ . $S_g \subset I_g$ . p. 7
$S_L, S_R$	private inner nodes originated from the left child cluster and right cluster, p. 13
$s, b$	size of the set $S$ and $B$ , p. 10
$N, N_x, N_y$	size of the mesh from the discretization of 2D device, p. 4. For square mesh, $N_x = N_y$ and we write it as $N$ , p. 8.
$n$	size of square matrices $\mathbf{A}$ , $\mathbf{\Sigma}$ , $\mathbf{G}$ , and $\mathbf{G}^<$ . For an $N_x \times N_y$ mesh, $n = N_x N_y$ . p. 4
$\mathbf{A}, \mathbf{A}^\dagger$	the sparse matrix from the discretization of the device and its conjugate transpose, p. 3
$\mathbf{G}^r, \mathbf{G}^<$	matrix associated with the retarded Green's function p. 3
$\mathbf{\Sigma}$	matrix associated with the self energy, p. 3
$\mathbf{L}, \mathbf{U}$	the LU factors of the sparse matrix $\mathbf{A}$ , p. 4
$\mathbf{L}_g$	we decompose the LU factorization of $\mathbf{A}$ into multiple partial factorizations: $\mathbf{L} = \prod_g \mathbf{L}_g$ . p. 4
$\mathbf{A}_g, \mathbf{A}_{g+}$	the matrices in the elimination process right before and after eliminating $S_g$ , respectively. p. 7
$\mathbf{\Sigma}_g, \mathbf{\Sigma}_{g+}$	we keep updating $\mathbf{\Sigma}$ as we factorize $\mathbf{A}$ and use a subscript to indicate the stage in the process.
$\mathcal{L}, \mathcal{L}_g$	$\mathcal{L}_g = \mathbf{L}_g(B_g, S_g)$ is the only non-zero off-diagonal block of $\mathbf{L}_g$ used for the update step for eliminating $S_g$ . Sometime it is simplified as $\mathcal{L}$ when the subscript $g$ is not important. p. 7
$\mathcal{U}, \mathcal{U}_g$	$\mathcal{U}_g$ is a simplified notation for $\mathbf{A}_{g+}(B_g, B_g)$ . We keep computing $\mathcal{U}_g$ when we calculate $\mathbf{G}^r$ . Sometimes $\mathcal{U}_g$ is further simplified as $\mathcal{U}$ when the subscript $g$ is not important. p. 7
$\mathcal{R}, \mathcal{R}_g$	$\mathcal{R}_g$ is a simplified notation for $\mathbf{\Sigma}_{g+}(B_g, B_g)$ . We keep computing $\mathcal{R}_g$ when we calculate $\mathbf{G}^<$ . Sometimes $\mathcal{R}_g$ is further simplified as $\mathcal{R}$ when the subscript $g$ is not important. p. 9

---

# 1 Introduction

In recent years, the non equilibrium Green's function formalism [1, 2, 3, 4] (NEGF) has been widely used to study the properties of nanoscale MOS (metal-oxide-semiconductor) transistors as well as nanowires and molecular electronic devices in which quantum effects are important. This formalism leads to the definition of two types of Green's function, the retarded Green's function and less-than Green's function. Their discretized approximations satisfy the following equations [5]:

$$\begin{aligned}\mathbf{A} &= \mathbf{H}_0(\mathcal{E}) + \mathbf{\Sigma}^r(\mathcal{E}) \\ \mathbf{G}^r(\mathcal{E}) &= \mathbf{A}^{-1} \\ \mathbf{G}^<(\mathcal{E}) &= \mathbf{G}^r(\mathcal{E}) \mathbf{\Sigma}(\mathcal{E}) [\mathbf{G}^r]^\dagger(\mathcal{E})\end{aligned}$$

where  $\mathcal{E}$  is the energy,  $\mathbf{H}_0$  is the Hamiltonian representing a single particle,  $\mathbf{\Sigma}^r$  is the self-energy used to model the contact of the nano-device (nano-transistors) with the (infinite) source and drain, and  $[\mathbf{G}^r]^\dagger$  is the conjugate transpose of  $\mathbf{G}^r$ .  $\mathbf{\Sigma}$  is the scattering self-energy matrix. It is typically assumed that  $\mathbf{\Sigma}$  is a diagonal matrix, even though we will see later on that this assumption can be relaxed for our approach. The charge density can be obtained from the diagonal entries of  $\mathbf{G}^<(\mathcal{E})$ . In a typical calculation, one needs to solve a coupled Schrödinger-Poisson system of equations using some iterative scheme. Each calculation of the diagonal of  $\mathbf{G}^<(\mathcal{E})$  is relatively fast, however the total computational cost can be very large since the charge density needs to be computed at all energy levels  $\mathcal{E}$ , and at each iteration of the Schrödinger-Poisson equation solver.

In this paper, we will focus on discretization schemes for the Hamiltonian operator  $\mathbf{H}_0$  that use a 2D Cartesian grid. The method can be extended to more general schemes including finite-element but the description is easier in the context of Cartesian grids. We will further assume that a 5 point finite-difference stencil is used, although the method can be extended to arbitrary stencils. This stencil is the most common for these types of problems. Finally even though the matrix is not symmetric we require that  $\mathbf{A}_{ij} \neq 0 \Leftrightarrow \mathbf{A}_{ji} \neq 0$ . All these requirements can be removed but these assumptions will simplify the discussion of the method.

In previous publications [6, 7, 5], we discussed an efficient method, FIND (Fast Inverse using Nested Dissection), to calculate the diagonal of  $\mathbf{G}^r = \mathbf{A}^{-1}$ . The novel contributions in this paper include:

- Extension of FIND [6, 7, 5] for computing the diagonal of  $\mathbf{G}^< = \mathbf{A}^{-1} \mathbf{\Sigma} \mathbf{A}^{-\dagger}$ . See Section 3.1.
- Extension for computing the off-diagonal entries of  $\mathbf{G}^r$ . This is required for computing the current density (see for example [8], eq. (20) pp 7847). This is presented in Section 3.2.
- Optimizations using certain sparsity patterns in  $\mathbf{A}$  to further reduce the computational cost (Section 4.1).
- Optimizations using the symmetry of  $\mathbf{A}$  (Section 4.2).
- Optimizations specific to computing the off-diagonal entries for current density calculations.
- Proof of symmetry and/or positive definiteness for matrices arising in the algorithm, when  $\mathbf{A}$  is itself symmetric and/or positive definite. See 4.2.
- Detailed analysis of the computational cost and storage requirement for the different approaches.

Pseudo-codes are given for the key algorithms. Numerical results with accuracy and performance benchmarks are given at the end (Section 5). The performance improvements vary but are on the order of 2x in general. In the appendix, we derive a series of technical results that are required to prove some of the statements in this paper.

Before beginning, we make some general comments regarding our approach and how it relates to other techniques. In [9, 10], methods are proposed to calculate the inverse of a dense matrix, of size  $N \times N$ , in

$O(N \ln^2 N)$  steps using low rank approximations of certain off-diagonal blocks. Similar techniques include  $\mathcal{H}^2$ -matrices, quasi-separable matrices, semi-separable matrices, and HSS-matrices [9, 11, 12, 13]. Mamaluy et al.’s method uses the special dependency of the problem on  $\mathcal{E}$  to reduce the computational cost [14, 15, 16, 17, 18, 19]. This last method requires computing the eigenvectors and eigenvalues of the decoupled Hamiltonian. In [20], a method is proposed in cases where the inverse matrix exhibits a decay property, i.e., when many of the entries of the inverse are small. In this paper, we seek to find exact methods that do not require special matrix properties or solving an eigenvalue problem.

An efficient approach in this second class of methods is the recursive Green’s function (RGF) method [21] (see also the earlier work of Erisman et al. [22]) with running time of order  $\mathcal{O}(N_x^3 N_y)$ , where  $N_x$  and  $N_y$  are the number of points on the grid in the  $x$  and  $y$  direction after discretization, respectively ( $N_x < N_y$ ). This technique was generalized in [23] to block tri-diagonal matrices. RGF type methods perform a forward recurrence, based on LU factorizations. This produces a single entry in the inverse. From this entry, a backward recurrence progressively computes the remaining entries. In contrast, FIND [6, 7, 5] performs two elimination passes, based on LU factorizations, typically described as upward elimination (similar to the LU factorization in RGF), and a downward elimination (which has no equivalent in RGF). At the end of the process, the inverse is directly computed as a by-product of the downward elimination. The work of Lin et al. [24, 25] follows an approach similar to FIND.

As a note, we mention that the algorithm presented below uses a decomposition of the problem based on nested dissection. The original nested dissection of George et al. [26], which is used to solve linear systems, requires defining **separator sets**. A separator set is a set of mesh nodes such that it divides the mesh in two sets  $C_1$  and  $C_2$ , and  $\mathbf{A}_{ij} = 0$  if  $i \in C_1$  and  $j \in C_2$ . An important difference between nested dissection and FIND is that, in the original nested dissection, a separator set is “shared” by the neighboring clusters. In FIND, since we need more independence among clusters, each cluster has its own boundary set that separates it from other clusters. These boundary sets are similar to the separator sets (generally called width-1 separators) used in nested dissection, but form so-called width-2 separators, with basically one “separator” for each of the two neighboring clusters. See for example [27, 28, 29, 30] for a definition of width- $l$  separators. Width- $l$  separators with  $l > 1$  are sometimes called wide separators. However, it is possible to construct a FIND algorithm that uses the more classical width-1 separators. Currently, FIND belongs to the class of **right-looking** algorithms (see [31] page 426, 427). A variant of FIND requiring only width-1 separators can be created using a **left-looking** strategy for the additions.<sup>1</sup> Even though the latter might be more efficient, in this paper, we focus on the original FIND scheme, which uses a right-looking approach with width-2 separators.

## 2 Previous work

### 2.1 Brief description of the FIND algorithm for $\mathbf{G}^r = \mathbf{A}^{-1}$

The basic idea of the FIND algorithm is to simultaneously perform many LU factorizations on the given matrix to obtain the diagonal elements of its inverse. By performing the LU factorizations in a specific order that minimizes fill-ins [26], we preserve most of the sparsity of the given matrix  $\mathbf{A}$ , and thus make the LU factorizations very efficient. Once an LU factorization is complete, we can easily compute the last entry on the diagonal of the inverse: for an  $n \times n$  matrix  $(\mathbf{G}^r)^{-1} = \mathbf{L}\mathbf{U}$ , we have  $\mathbf{G}_{nn}^r = 1/\mathbf{U}_{nn}$ . Although we can compute only the  $(n, n)$  entry of the diagonal by this formula, we can choose any node and reorder the original matrix to make that node correspond to the  $(n, n)$  entry of the reordered matrix. In this way, all the diagonal elements of  $\mathbf{G}^r$  can be computed.

If we have to perform a full LU factorization for each of the  $n$  reordered matrices, the algorithm will not be computationally efficient even though each LU factorization is very fast. However, we can decompose each LU factorization into partial LU factorizations:  $\mathbf{A} = \prod_g \mathbf{L}_g \prod_g \mathbf{U}_g$ , where  $\mathbf{L}_g$  corresponds to the elimination of  $S_g$  and  $S_g$  is a set of private inner nodes that we will discuss in Section 2.2. Due to the sparsity pattern of  $\mathbf{A}$ , we can perform them independently and moreover, if we reorder  $\mathbf{A}$  properly, many partial factorizations

---

<sup>1</sup>Specifically, this variant uses right-looking multiplications and left-looking additions.

for different reordered matrices turn out to be identical. As a result, we can reuse the partial results multiple times for different orderings thereby reducing considerably the computational cost.

More specifically, we partition the mesh into subsets of mesh nodes. Fig. 1(a) shows the partitions of the entire mesh into 2, 4, and 8 clusters, for a 2D rectangular grid. Then, these subsets are merged to form larger clusters. Each merge corresponds to a partial Gaussian elimination. The clusters shown on the left panel 1(a) are called *basic clusters* and usually denoted as  $C$ . They are labeled with positive integers therefore sometimes called *positive clusters*. For reasons we will see soon, we also consider the complement of the basic clusters with respect to the whole mesh  $M$ . These clusters are called *complement clusters* and denoted as  $\bar{C}$ . They are labeled with negative integers therefore sometimes called *negative clusters* as shown in Fig. 1(b).

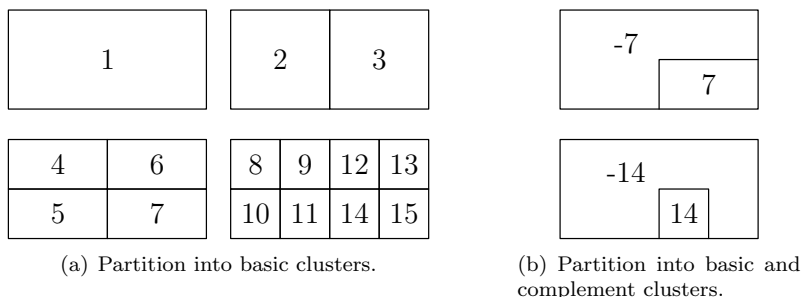


Figure 1: Partitions of a 2D rectangular mesh into clusters

We organize these basic and complement clusters in trees to see how the partial eliminations are related to the full elimination. Fig. 2(a) shows how the basic clusters form a *basic cluster tree*, usually denoted as  $T$ . For each of the leaf clusters (*target cluster*) in the figure, we order the matrix  $\mathbf{A}$ , such that the entries corresponding to the target cluster (*target entries*) form a block at the end of the matrix. We then eliminate all the columns corresponding to the complement of the target cluster to compute the target entries in  $\mathbf{A}^{-1}$ .

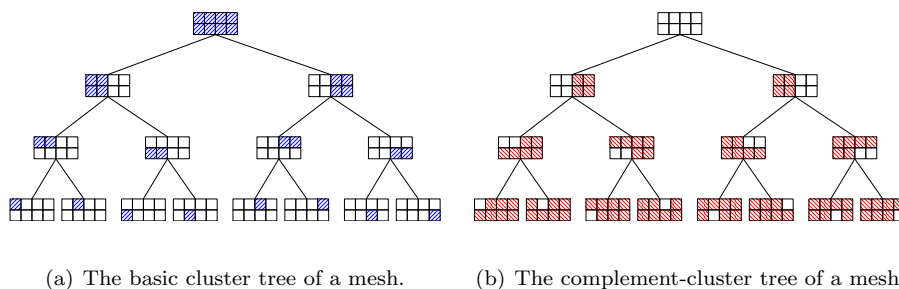


Figure 2: Cluster trees.

Because the complements of the target clusters overlap significantly, we organize these clusters, together with other complement clusters, into a similar *complement cluster tree*, as shown in Fig. 2(b). Unlike the clusters in Fig. 2(a), a parent cluster in Fig. 2(b) is not a union of its two child clusters, but rather their intersection.

The two cluster trees in Fig. 3 show how two leaf complement clusters  $-14$  and  $-15$  are computed by the FIND algorithm. Such trees are called *augmented trees* and are denoted as  $T_r^+$  with  $r$  indicating the target cluster, i.e., the complement of the root cluster. Each tree is associated with an ordering of  $\mathbf{A}$  with the target entries appearing at the end of the matrix. The path  $(-3)-(-7)-(-14)$  in  $T_{14}^+$  and the path  $(-3)-(-7)-(-15)$

in  $T_{15}^+$  are part of the complement-cluster tree; the other subtrees are copies from the basic cluster tree. We can see that these two trees are almost identical, which means that the two full LU factorizations of  $\mathbf{A}$  with different orderings significantly overlap.

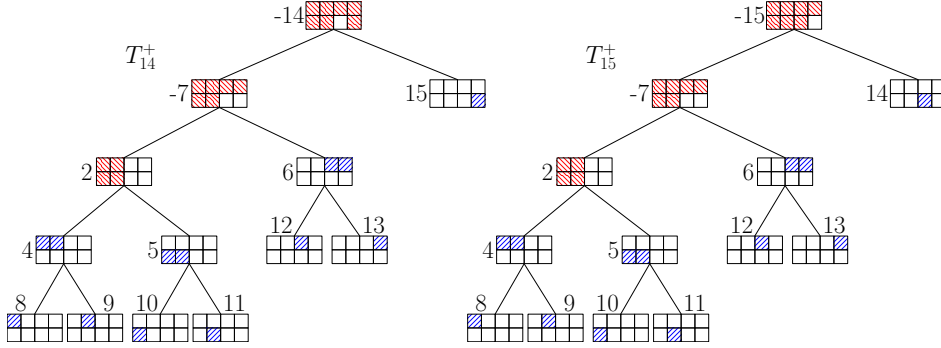


Figure 3: Two augmented trees with target clusters 14 and 15.

At each level of the two trees, two clusters are merged into a larger one. We define the *inner nodes* of a cluster  $C$  as the subset of nodes  $l$  in a cluster such that  $\mathbf{A}_{ij} = 0$  for any  $i \in l$  and  $j \notin C$ . Each merge is equivalent to the Gaussian elimination of all the inner nodes of the resulting cluster. For example, in Fig. 4, the large cluster has been surrounded by a solid line with tics. The two children clusters are on the left and right. During earlier steps in the method, the  $\times$  nodes have been eliminated. At the current step, the  $\circ$  nodes are being eliminated. As a result, all the inner nodes of the clusters have been eliminated at the end of this operation.

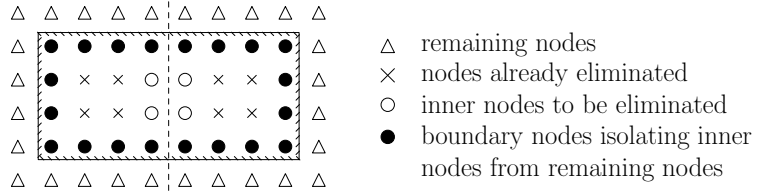


Figure 4: The nodes within the rectangular frame form a large cluster. Two child clusters are shown on the left and right.

Such a merge corresponds to an independent partial LU factorization since there is no connection between the eliminated nodes ( $\circ$ ) and the remaining nodes ( $\Delta$ ). This is better seen below in the Gaussian elimination in (1) for the merge in Fig. 4:

$$\begin{pmatrix} \mathbf{A}(\circ, \circ) & \mathbf{A}(\circ, \bullet) & \mathbf{0} \\ \mathbf{A}(\bullet, \circ) & \mathbf{A}(\bullet, \bullet) & \mathbf{A}(\bullet, \Delta) \\ \mathbf{0} & \mathbf{A}(\Delta, \bullet) & \mathbf{A}(\Delta, \Delta) \end{pmatrix} \Rightarrow \begin{pmatrix} \mathbf{A}(\circ, \circ) & \mathbf{A}(\circ, \bullet) & \mathbf{0} \\ \mathbf{0} & \mathbf{A}^*(\bullet, \bullet) & \mathbf{A}(\bullet, \Delta) \\ \mathbf{0} & \mathbf{A}(\Delta, \bullet) & \mathbf{A}(\Delta, \Delta) \end{pmatrix}, \quad (1)$$

where  $\mathbf{A}^*(\bullet, \bullet) = \mathbf{A}(\bullet, \bullet) - \mathbf{A}(\bullet, \circ)\mathbf{A}(\circ, \circ)^{-1}\mathbf{A}(\circ, \bullet)$

In (1),  $\circ$  and  $\bullet$  each corresponds to all the  $\circ$  nodes and  $\bullet$  nodes in Fig. 4, respectively.  $\mathbf{A}^*(\bullet, \bullet)$  is the result of the partial LU factorization. It will be stored for reuse when we go through the cluster trees.

To make the most of the overlap, we do not perform the eliminations for each augmented tree individually. Instead, we perform the elimination based on the basic cluster tree and the complement-cluster tree in the FIND algorithm. We start by eliminating all the inner nodes of the leaf clusters in Fig. 2(a) followed by eliminating the inner nodes of their parents recursively until we reach the root cluster. This is called the

*upward pass*. Once we have the partial elimination results from upward pass, we can use them to traverse the complement-cluster tree level by level, from the root to the leaf clusters. This is called the *downward pass*.

## 2.2 Formal description of the FIND algorithm

Section 2.1 briefly illustrated how the algorithm works by showing that the eliminations of inner nodes are independent of each other (Eq. (1)) and such eliminations are mostly shared among different augmented trees (Fig. 3). Below we will show in a more formal way why the basic FIND algorithm works.

In Fig. 4, the  $\bullet$  nodes are called the boundary nodes, denoted as  $B_i$ . The inner nodes consist of the  $\circ$  and  $\times$  nodes, denoted as  $I_i$ . We call the  $\circ$  nodes *private inner nodes* and denote them as  $S_i$ . Private inner nodes are the nodes that actually get eliminated when we process the cluster. To guarantee the independence of the eliminations shown by (1) and the overlap of the eliminations for different target nodes illustrated by Fig. 3, we need to order the original matrix  $\mathbf{A}$  such that all the columns corresponding to the private nodes of each cluster in Fig. 1 are grouped together. It can be shown that for each target cluster, the whole mesh can be partitioned as a series of sets of private inner nodes ( $S_i$ ), the set of boundary nodes  $B_{\bar{r}}$  of the complement of the target cluster, and the target cluster  $C_r$ . We order the columns in  $\mathbf{A}$  based on the ordering of these sets:  $S_i$  of the leaf clusters first, followed by  $S_i$  of their parents,  $S_i$  of the clusters in the next level in the augmented tree,  $\dots$ ,  $S_{\bar{r}}$ ,  $B_{\bar{r}}$ , and finally  $C_r$ . We call such ordering a *consistent ordering* with respect to a target cluster. Note that the consistent ordering is not unique since we do not require any specific ordering of clusters at the same level in the augmented tree. Here is an example of a consistent ordering with respect to the target cluster 14:  $S_8, S_9, S_{10}, S_{11}, S_4, S_5, S_{12}, S_{13}, S_{\bar{3}}, S_6, S_{\bar{7}}, S_{15}, S_{\bar{14}}, B_{\bar{14}}$ , and  $C_{14}$ .

For notation convenience, we write  $S_i < S_j$  if  $S_i$  appears before  $S_j$  in a ordering and write  $\cup_{S_j < S_i} S_j$  as  $S_{<i}$  and  $(\cup_{S_i < S_j} S_j) \cup B_{\bar{r}} \cup C_r$  as  $S_{>i}$ . We also denote as  $\mathbf{A}_g$  the matrix  $\mathbf{A}$  after all the columns corresponding to the private nodes appearing before  $S_g$  have been eliminated and denote as  $\mathbf{A}_{g+}$  the matrix with all the columns before and including  $S_g$  have been eliminated. When necessary, we write them as  $\mathbf{A}_{r,g}$  and  $\mathbf{A}_{r,g+}$  to indicate explicitly the target cluster  $r$  of the elimination process. Now, we can rewrite the one-step elimination illustrated by (1) more formally as:

$$\mathbf{A}_g = \begin{pmatrix} \mathbf{A}_g(S_{<g}, S_{<g}) & \mathbf{A}_g(S_{<g}, S_g) & \mathbf{A}_g(S_{<g}, B_g) & \mathbf{A}_g(S_{<g}, S_{>g} \setminus B_g) \\ \mathbf{0} & \mathbf{A}_g(S_g, S_g) & \mathbf{A}_g(S_g, B_g) & \mathbf{0} \\ \mathbf{0} & \mathbf{A}_g(B_g, S_g) & \mathbf{A}_g(B_g, B_g) & \mathbf{A}_g(B_g, S_{>g} \setminus B_g) \\ \mathbf{0} & \mathbf{0} & \mathbf{A}_g(S_{>g} \setminus B_g, B_g) & \mathbf{A}_g(S_{>g} \setminus B_g, S_{>g} \setminus B_g) \end{pmatrix}$$

$\Rightarrow$

$$\mathbf{A}_{g+} = \begin{pmatrix} \mathbf{A}_g(S_{<g}, S_{<g}) & \mathbf{A}_g(S_{<g}, S_g) & \mathbf{A}_g(S_{<g}, B_g) & \mathbf{A}_g(S_{<g}, S_{>g} \setminus B_g) \\ \mathbf{0} & \mathbf{A}_g(S_g, S_g) & \mathbf{A}_g(S_g, B_g) & \mathbf{0} \\ \mathbf{0} & \mathbf{0} & \mathbf{A}_{g+}(B_g, B_g) & \mathbf{A}_g(B_g, S_{>g} \setminus B_g) \\ \mathbf{0} & \mathbf{0} & \mathbf{A}_g(S_{>g} \setminus B_g, B_g) & \mathbf{A}_g(S_{>g} \setminus B_g, S_{>g} \setminus B_g) \end{pmatrix}$$

where

$$\mathbf{A}_{g+}(B_g, B_g) = \mathbf{A}_g(B_g, B_g) - \mathbf{A}_g(B_g, S_g) \mathbf{A}_g(S_g, S_g)^{-1} \mathbf{A}_g(S_g, B_g). \quad (2)$$

For notation simplicity, we write  $\mathbf{A}_{g+}(B_g, B_g)$  as  $\mathcal{U}_g$ . This is the block we keep computing in our algorithm. Also recall that  $\mathbf{A} = \prod_g \mathbf{L}_g \prod_g \mathbf{U}_g$ , where  $\mathbf{L}_g$  corresponds to the elimination of  $S_g$ . So we have  $\mathbf{A}_{g+} = \mathbf{L}_g^{-1} \mathbf{A}_g$  with  $\mathbf{L}_g^{-1}(B_g, S_g) = -\mathbf{L}_g(B_g, S_g) = -\mathbf{A}_g(B_g, S_g) \mathbf{A}_g(S_g, S_g)^{-1}$  the only non-zero off-diagonal block of  $\mathbf{L}_g$  (see Li et al. for more details) [5]. We can further define

$$\mathcal{L}_g = \mathbf{L}_g(B_g, S_g), \quad (3)$$

and then we can write (2) as

$$\mathbf{A}_{g+}(B_g, B_g) = \mathbf{A}_g(B_g, B_g) - \mathcal{L}_g \mathbf{A}_g(S_g, B_g). \quad (4)$$

Note that in the above matrices, for notation convenience,  $\mathbf{A}_g(\bullet, \mathbf{B}_g)$  is written as a block. In reality, however, it is usually not a block in  $\mathbf{A}$  of any ordering in our algorithm because the columns of  $\mathbf{A}$  are ordered based on  $\mathbf{S}_g$  but not  $\mathbf{B}_g$ . It can be shown that the matrix preserves the sparsity pattern required by the above formula during the elimination process, which leads to the following theorem:

**Theorem 1** *For any target clusters  $r$  and  $s$  such that  $\mathbf{C}_g \in \mathbb{T}_r^+$  and  $\mathbf{C}_g \in \mathbb{T}_s^+$ , we have*

$$\mathbf{A}_{r,g+}(\mathbf{B}_g, \mathbf{B}_g) = \mathbf{A}_{s,g+}(\mathbf{B}_g, \mathbf{B}_g).$$

Theorem 1 shows that the partial elimination results are common for matrices with different orderings during the elimination process. This is the key foundation of the basic FIND algorithm. For more details, please see [5].

### 2.3 Cost analysis of the FIND algorithm for $\mathbf{A}^{-1}$

For analytic simplicity, we assume that  $\mathbf{A}$  comes from a square grid of size  $N \times N$ . In this case, the total cost is  $\mathcal{O}(N^3)$ . This is the same computational cost in the  $\mathcal{O}$  sense as the nested dissection algorithm of George et al. [26]. It is now apparent that FIND has the same order of computational complexity as a single LU factorization, even though it calculates the diagonal of the inverse matrix.

Similar analysis tells us that the total memory cost is  $\mathcal{O}(N^2 \log(N))$ . Both costs are asymptotically better than those for the best known algorithm, RGF, given by Svizhenko et al. [21]. However, the constant factor in RGF [32] is smaller than ours [5]. As a result, with the chosen tree decomposition, we are slower than RGF for meshes smaller than  $130 \times 130$ . The single-layer-separator FIND variant discussed in the introduction would make FIND as fast as RGF even for small matrices. The following two sections will explain how to exploit the sparsity and symmetry to reduce the constant factor in FIND.

## 3 Extension of the FIND algorithm

In addition to computing the diagonal entries of the matrix inverse, the algorithm can be extended to computing the diagonal entries and certain off-diagonal entries of  $\mathbf{G}^< = \mathbf{A}^{-1}\mathbf{\Sigma}\mathbf{A}^{-\dagger}$ , which are required for the charge and current densities.

### 3.1 Computing the diagonal entries of $\mathbf{G}^<$

Intuitively,  $\mathbf{A}^{-1}\mathbf{\Sigma}\mathbf{A}^{-\dagger}$  can be computed in the same way as  $\mathbf{A}^{-1}$  because we have

$$\begin{aligned} \mathbf{G}^< &= \mathbf{A}^{-1}\mathbf{\Sigma}\mathbf{A}^{-\dagger} \\ \Rightarrow \mathbf{A}\mathbf{G}^<\mathbf{A}^\dagger &= \mathbf{\Sigma} \\ \Rightarrow \mathbf{U}\mathbf{G}^<\mathbf{U}^\dagger &= \mathbf{L}^{-1}\mathbf{\Sigma}\mathbf{L}^{-\dagger} \\ \Rightarrow [\mathbf{G}^<]_{nn} &= (\mathbf{U}_{nn})^{-1}(\mathbf{L}^{-1}\mathbf{\Sigma}\mathbf{L}^{-\dagger})_{nn}(\mathbf{U}_{nn})^{-\dagger}. \end{aligned} \tag{5}$$

Now, it remains to show how to compute  $(\mathbf{L}^{-1}\mathbf{\Sigma}\mathbf{L}^{-\dagger})_{nn}$  efficiently. In the appendix, we show that if we order  $\mathbf{\Sigma}$  in a same way as  $\mathbf{A}$ , the pattern of  $\mathbf{\Sigma}$  will be similar to that of  $\mathbf{A}$  during the update process. Therefore, we can decompose the computation for the last block of  $\mathbf{L}^{-1}\mathbf{\Sigma}\mathbf{L}^{-\dagger}$  into multiple steps with each step involving only a few small blocks. More specifically, we have a sequence of matrices  $\mathbf{\Sigma}_g$  that start from  $\mathbf{\Sigma}$  and end at  $(\mathbf{L}^{-1}\mathbf{\Sigma}\mathbf{L}^{-\dagger})_{nn}$ . This sequence is synchronized with the updates on  $\mathbf{A}$ , and similar to the update  $\mathbf{A}_{g+} = \mathbf{L}_g^{-1}\mathbf{A}_g$ , we have  $\mathbf{\Sigma}_{g+} = \mathbf{L}_g^{-1}\mathbf{\Sigma}_g\mathbf{L}_g^{-\dagger}$ . This one-step update is given by:

$$\mathbf{\Sigma}_g = \begin{pmatrix} \mathbf{\Sigma}_g(\mathbf{S}_{<g}, \mathbf{S}_{<g}) & \mathbf{\Sigma}_g(\mathbf{S}_{<g}, \mathbf{S}_g) & \frac{\mathbf{\Sigma}_g(\mathbf{S}_{<g}, \mathbf{B}_g)}{\mathbf{\Sigma}_g(\mathbf{S}_g, \mathbf{B}_g)} & \mathbf{\Sigma}_g(\mathbf{S}_{<g}, \mathbf{S}_{>g} \setminus \mathbf{B}_g) \\ \mathbf{\Sigma}_g(\mathbf{S}_g, \mathbf{S}_{<g}) & \mathbf{\Sigma}_g(\mathbf{S}_g, \mathbf{S}_g) & \frac{\mathbf{\Sigma}_g(\mathbf{S}_g, \mathbf{B}_g)}{\mathbf{\Sigma}_g(\mathbf{B}_g, \mathbf{B}_g)} & \mathbf{0} \\ \mathbf{\Sigma}_g(\mathbf{B}_g, \mathbf{S}_{<g}) & \mathbf{\Sigma}_g(\mathbf{B}_g, \mathbf{S}_g) & \frac{\mathbf{\Sigma}_g(\mathbf{B}_g, \mathbf{B}_g)}{\mathbf{\Sigma}_g(\mathbf{S}_{>g} \setminus \mathbf{B}_g, \mathbf{B}_g)} & \mathbf{\Sigma}_g(\mathbf{B}_g, \mathbf{S}_{>g} \setminus \mathbf{B}_g) \\ \mathbf{\Sigma}_g(\mathbf{S}_{>g} \setminus \mathbf{B}_g) & \mathbf{0} & \mathbf{\Sigma}_g(\mathbf{S}_{>g} \setminus \mathbf{B}_g, \mathbf{B}_g) & \mathbf{\Sigma}_g(\mathbf{S}_{>g} \setminus \mathbf{B}_g, \mathbf{S}_{>g} \setminus \mathbf{B}_g) \end{pmatrix} \tag{6}$$



$\Rightarrow$

$$\Sigma_{g+} = \begin{pmatrix} \Sigma_g(S_{<g}, S_{<g}) & \Sigma_g(S_{<g}, S_g) & \Sigma_{g+}(S_{<g}, B_g) & \Sigma_g(S_{<g}, S_{>g} \setminus B_g) \\ \Sigma_g(S_g, S_{<g}) & \Sigma_g(S_g, S_g) & \Sigma_{g+}(S_g, B_g) & \mathbf{0} \\ \Sigma_{g+}(B_g, S_{<g}) & \Sigma_{g+}(B_g, S_g) & \Sigma_{g+}(B_g, B_g) & \Sigma_g(B_g, S_{>g} \setminus B_g) \\ \Sigma_g(S_{>g} \setminus B_g) & \mathbf{0} & \Sigma_g(S_{>g} \setminus B_g, B_g) & \Sigma_g(S_{>g} \setminus B_g, S_{>g} \setminus B_g) \end{pmatrix},$$

where

$$\begin{aligned} \Sigma_{g+}(B_g, B_g) &= \Sigma_g(B_g, B_g) - \mathcal{L}_g \Sigma_g(S_g, B_g) \\ &\quad - \Sigma_g(B_g, S_g) \mathcal{L}_g^\dagger + \mathcal{L}_g \Sigma_g(S_g, S_g) \mathcal{L}_g^\dagger, \end{aligned} \quad (7)$$

The difference between the updates on  $\mathbf{A}$  and the updates on  $\Sigma$  is that the latter will not only change  $\Sigma_g(B_g, B_g)$ , but also  $\Sigma_g(S_{\leq g}, B_g)$  and  $\Sigma_g(B_g, S_{\leq g})$ . These blocks are underlined in (6). The reason for these changes is that we multiply  $\Sigma$  by  $\mathbf{L}^{-1}$  from both sides and the subdiagonal blocks of  $\Sigma_g$  are not cleared through the update process. The changes to  $\Sigma_g(S_{\leq g}, B_g)$  and  $\Sigma_g(B_g, S_{\leq g})$ , however, do not invalidate the update process because in any future update step  $h > g$ , we are only interested in the operation on the submatrix  $\Sigma_h(S_{\geq h}, S_{\geq h})$  and  $S_{\leq g} \cap S_{\geq h} = \emptyset$ . See the appendix for a rigorous description and proof.

Note that even though  $\Sigma_{r,g+}$  generally depends on  $r$  (corresponding to the ordering for different target clusters),  $\Sigma_{r,g+}(B_g, B_g)$  does not, as shown in the appendix. For notation simplicity, we write  $\Sigma_{g+}(B_g, B_g)$  as  $\mathcal{R}_g$ . The major part of the computation for  $\mathbf{G}^<$  is to compute  $\mathcal{R}_g$  (for  $\mathbf{G}^<$ ), along with  $\mathcal{U}_g$  (for both  $\mathbf{G}^r$  and  $\mathbf{G}^<$ ), for all clusters.

### 3.1.1 The algorithm and pseudo-codes

Let  $C_i$  and  $C_j$  be the two children of  $C_g$  in  $\mathbb{T}_r^+$ . To compute  $\mathcal{R}_g$ , we need both  $\mathbf{A}_g(S_g \cup B_g, S_g \cup B_g)$  and  $\Sigma_g(S_g \cup B_g, S_g \cup B_g)$ .  $\mathbf{A}_g(S_g \cup B_g, S_g \cup B_g)$  follows the same update rule as in the basic FIND algorithm; and  $\Sigma_g(S_g \cup B_g, S_g \cup B_g)$  is given by the following four blocks:

$$\begin{aligned} \Sigma_g(S_g, S_g) &= \begin{pmatrix} \Sigma_i(S_g \cap B_i, S_g \cap B_i) & \Sigma(S_g \cap B_i, S_g \cap B_j) \\ \Sigma(S_g \cap B_j, S_g \cap B_i) & \Sigma_j(S_g \cap B_j, S_g \cap B_j) \end{pmatrix}, \\ \Sigma_g(S_g, B_g) &= \begin{pmatrix} \Sigma_i(S_g \cap B_i, B_g \cap B_i) & \mathbf{0} \\ \mathbf{0} & \Sigma_j(S_g \cap B_j, B_g \cap B_j) \end{pmatrix}, \\ \Sigma_g(B_g, S_g) &= \begin{pmatrix} \Sigma_i(B_g \cap B_i, S_g \cap B_i) & \mathbf{0} \\ \mathbf{0} & \Sigma_j(B_g \cap B_j, S_g \cap B_j) \end{pmatrix}, \end{aligned}$$

and

$$\Sigma_g(B_g, B_g) = \begin{pmatrix} \Sigma_i(B_g \cap B_i, B_g \cap B_i) & \Sigma(B_g \cap B_i, B_g \cap B_j) \\ \Sigma(B_g \cap B_j, B_g \cap B_i) & \Sigma_j(B_g \cap B_j, B_g \cap B_j) \end{pmatrix}.$$

To compute  $\mathbf{G}^<$ , we start from the given  $\mathbf{A}$  and  $\Sigma$  and keep applying the update rule (7). Similar to the basic FIND algorithm, if  $C_g$  is a leaf node, then we have  $\Sigma_g(B_g \cup S_g, B_g \cup S_g) = \Sigma(B_g \cup S_g, B_g \cup S_g)$ , i.e., we can use the entries in the original  $\Sigma$  (see appendix). The recursive process of updating  $\Sigma$  is the same as updating  $\mathbf{A}$  in the basic FIND algorithm, but the update rule is different here.

The pseudocode of the algorithm is an extension of the basic FIND algorithm. In addition to rearranging  $\mathbf{A}$  and computing matrices  $\mathcal{U}_g$ , we need to perform similar operations for  $\Sigma$  and compute matrices  $\mathcal{R}_g$ . Note that even if we do not need  $\mathbf{A}^{-1}$ , we still need to keep track of the update of  $\mathbf{A}$ , i.e., the  $\mathcal{U}$  matrices. This is because we need  $\mathbf{A}_g(B_g \cup S_g, B_g \cup S_g)$  to update  $\Sigma_g(B_g, B_g)$  and obtain  $\mathcal{R}_g$ . Once we have prepared  $\mathcal{R}_g$  for all the positive clusters, we can compute  $\mathcal{R}_g$  for the negative clusters. This is done in the downward pass as shown in the procedure `updateAdjacentNodes` below. The whole algorithm is shown in procedure `computeG<`. In these procedures, we use slightly different notations. Instead of using  $C_g$ ,  $B_g$ , and  $S_g$  for the sets of boundary nodes and private inner nodes, we use  $C$ ,  $B_C$ , and  $S_C$ . We also use  $\mathcal{U}_C$  and  $\mathcal{R}_C$  for the corresponding  $\mathcal{U}_g$  and  $\mathcal{R}_g$ , respectively.

---

**Procedure** updateBoundaryNodes(cluster C). This procedure is called with the root of the tree: updateBoundaryNodes(root).

---

**Data:** tree decomposition of the mesh; the matrix  $\mathbf{A}$ .

**Input:** cluster C with  $n$  boundary mesh nodes.

**Output:** all the inner mesh nodes of cluster C are eliminated by the procedure. The  $n \times n$  matrices  $\mathcal{U}_C$  for  $\mathbf{G}^r$  and  $\mathcal{R}_C$  for  $\mathbf{G}^<$  are computed and saved.

```

1 if C is not a leaf then
2   C1 = left child of C;
3   C2 = right child of C;
4   updateBoundaryNodes(C1)           /* The boundary set is denoted BC1 */;
5   updateBoundaryNodes(C2)           /* The boundary set is denoted BC2 */;
6 else
7    $\mathbf{A}_C = \mathbf{A}(C, C)$ ;
8 if C is not the root then
9    $\mathbf{A}_C = [\mathcal{U}_{C1} \mathbf{A}(B_{C1}, B_{C2}); \mathbf{A}(B_{C2}, B_{C1}) \mathcal{U}_{C2}]$ ;
   /*  $\mathbf{A}(B_{C1}, B_{C2})$  and  $\mathbf{A}(B_{C2}, B_{C1})$  are values from the original matrix  $\mathbf{A}$ . */
10  Rearrange  $\mathbf{A}_C$  such that the inner nodes of  $B_{C1} \cup B_{C2}$  appear first;
11  Set  $S_g$  in Eq. (7) to be the above inner nodes and  $B_g$  the rest;
12  Eliminate the inner nodes to compute  $\mathcal{U}_C$  by Eq. (2);
13   $\Sigma_C = [\Sigma_{C1} \Sigma(B_{C1}, B_{C2}); \Sigma(B_{C2}, B_{C1}) \Sigma_{C2}]$ ;
   /*  $\Sigma(B_{C1}, B_{C2})$  and  $\Sigma(B_{C2}, B_{C1})$  are values from the original matrix  $\Sigma$ . */
14  Rearrange  $\Sigma_C$  in the same way as  $\mathbf{A}_C$ ;
15  Compute  $\mathcal{R}_C$  based on Eq. (7);
16  Save  $\mathcal{U}_C$  and  $\mathcal{R}_C$ ;

```

---

### 3.1.2 Computation and storage cost

Similar to the computation cost analysis in [5], the major computation cost comes from computing (7).

The cost depends on the size of  $S_g$  and  $B_g$ . Let  $s = |S_g|$  and  $b = |B_g|$  be the sizes, then the computation cost for  $\mathcal{L}_g \Sigma_g(S_g, B_g)$  is  $(\frac{1}{3}s^3 + s^2b + sb^2)$  flops. Since  $\mathcal{L}_g$  is already given in (2), the cost is reduced to  $sb^2$ . Similarly, the cost for  $\Sigma_g(B_g, S_g) \mathcal{L}_g^\dagger$  is also  $sb^2$  and the cost for  $\mathcal{L}_g \Sigma_g(S_g, S_g) \mathcal{L}_g^\dagger$  is  $sb^2 + s^2b$ . So the total cost for (7) is  $(3sb^2 + s^2b)$  flops. Note that these cost estimates need explicit form of  $\mathbf{A}(B, S) \mathbf{A}(S, S)^{-1}$  and we need to arrange the order of computation to have it as an intermediate result in computing (2).

Now we consider the whole process. We analyze the cost in the two passes.

For the upward pass, when two  $(a \times a)$ -clusters merge into one  $(a \times 2a)$ -cluster,  $b \leq 6a$  and  $s \leq 2a$ , so the cost is at most  $360a^3$  flops; when two  $(a \times 2a)$ -clusters merge into one  $(2a \times 2a)$ -cluster,  $b \leq 8a$  and  $s \leq 4a$ , so the cost is at most  $896a^3$  flops. We have  $\frac{N_x N_y}{2a^2}$   $(a \times 2a)$ -clusters and  $\frac{N_x N_y}{4a^2}$   $(2a \times 2a)$ -clusters, so the cost for these two levels is  $(360a^3 \frac{N_x N_y}{2a^2} + 896a^3 \frac{N_x N_y}{4a^2}) = 404N_x N_y a$ . Sum all the levels together up to  $a = N_x/2$ , the computation cost for upward pass is then  $404N_x^2 N_y$ .

For the downward pass, when one  $(2a \times 2a)$ -cluster is partitioned to two  $(a \times 2a)$ -clusters,  $b \leq 6a$  and  $s \leq 8a$ , so the cost is at most  $1248a^3$  flops; when one  $(a \times 2a)$ -cluster is partitioned to two  $(a \times a)$ -clusters,  $b \leq 4a$  and  $|S_g| \leq 6a$ , so the cost is at most  $432a^3$  flops. We have  $\frac{N_x N_y}{2a^2}$   $(a \times 2a)$ -clusters and  $\frac{N_x N_y}{a^2}$   $(a \times a)$ -clusters, so the cost for these two levels is  $(1248a^3 \frac{N_x N_y}{2a^2} + 432a^3 \frac{N_x N_y}{a^2}) = 1056N_x N_y a$ . Sum all the levels together up to  $a = N_x/2$ , the computation cost for downward pass is then at most  $1056N_x^2 N_y$ .

## 3.2 Computing off-diagonal entries of $\mathbf{G}^r$ and $\mathbf{G}^<$

In addition to computing the diagonal entries of  $\mathbf{G}^r$  and  $\mathbf{G}^<$ , the algorithm can also be easily extended to computing the entries in  $\mathbf{G}^r$  and  $\mathbf{G}^<$  corresponding to neighboring nodes. These entries are often of interest

---

**Procedure** updateAdjacentNodes(cluster C). This procedure is called with the root of the tree: updateAdjacentNodes(root).

---

**Data:** tree decomposition of the mesh; the matrix  $\mathbf{A}$ ; the upward pass [updateBoundaryNodes()] should have been completed.

**Input:** cluster C with  $n$  adjacent mesh nodes (as the boundary nodes of  $\bar{C}$ ).

**Output:** all the outer mesh nodes of cluster C (as the inner nodes of  $\bar{C}$ ) are eliminated by the procedure. The  $n \times n$  matrices  $\mathcal{U}_{\bar{C}}$  and  $\mathcal{R}_{\bar{C}}$  are computed and saved.

```

1 if C is not the root then
2   D = parent of C           /* The boundary set of  $\bar{D}$  is denoted  $B_{\bar{D}}$  */;
3   D1 = sibling of C         /* The boundary set of D1 is denoted  $B_{D1}$  */;
4    $\mathbf{A}_{\bar{C}} = [\mathcal{U}_{\bar{D}} \mathbf{A}(B_{\bar{D}}, B_{D1}); \mathbf{A}(B_{D1}, B_{\bar{D}}) \mathcal{U}_{D1}]$ ;
   /*  $\mathbf{A}(B_{\bar{D}}, B_{D1})$  and  $\mathbf{A}(B_{D1}, B_{\bar{D}})$  are values from the original matrix A. */
   /* If D is the root, then  $\bar{D} = \emptyset$  and  $\mathbf{A}_{\bar{C}} = \mathbf{R}_{D1}$ . */
5   Rearrange  $\mathbf{A}_{\bar{C}}$  such that the inner nodes of  $B_{\bar{D}} \cup B_{D1}$  appear first;
6   Set  $S_g$  in Eq. (7) to be the above inner nodes and  $B_g$  the rest;
7   Eliminate the outer nodes to compute  $\mathcal{U}_{\bar{C}}$  by Eq. (2);
8    $\Sigma_{\bar{C}} = [\mathcal{R}_{\bar{D}} \Sigma(B_{\bar{D}}, B_{D1}); \Sigma(B_{D1}, B_{\bar{D}}) \mathcal{R}_{D1}]$ ;
9   Rearrange  $\Sigma_{\bar{C}}$  in the same way as for  $\mathbf{A}_{\bar{C}}$ ;
10  Compute  $\mathcal{R}_{\bar{C}}$  based on Eq.(7);
11  Save  $\mathcal{U}_{\bar{C}}$  and  $\mathcal{R}_{\bar{C}}$ ;
12 if C is not a leaf then
13   C1 = left child of C;
14   C2 = right child of C;
15   updateAdjacentNodes(C1);
16   updateAdjacentNodes(C2);

```

---



---

**Procedure** compute $\mathbf{G}^<$ (mesh M). This procedure is called by any function that needs  $\mathbf{G}^<$  of the whole mesh.

---

**Input:** the mesh M; the matrix  $\mathbf{A}$ ; the matrix  $\Sigma$ .

**Output:** the diagonal entries of  $\mathbf{G}^<$ .

```

1 Prepare the tree decomposition of the whole mesh;
2 updateBoundaryNodes(root);
3 updateAdjacentNodes(root);
4 for each leaf node C do
5   Compute  $[\mathbf{A}^{-1}](C, C)$  using Eq. (8);
6   Compute  $\mathbf{G}_{\bar{C}}^<$  based on Eq. (5);
7   Save  $\mathbf{G}_{\bar{C}}^<$  together with its indices;
8 Collect  $\mathbf{G}_{\bar{C}}^<$  with their indices and output all the diagonal entries of  $\mathbf{G}^<$ ;

```

---

in simulation. For example, the current density can be computed using off-diagonal entries corresponding to horizontally neighboring nodes. These entries can be obtained with a slight modification of the algorithm. For simplicity, we only consider the off-diagonal entries of  $\mathbf{G}^r$ . The off-diagonal entries of  $\mathbf{G}^<$  can be treated in a similar way.

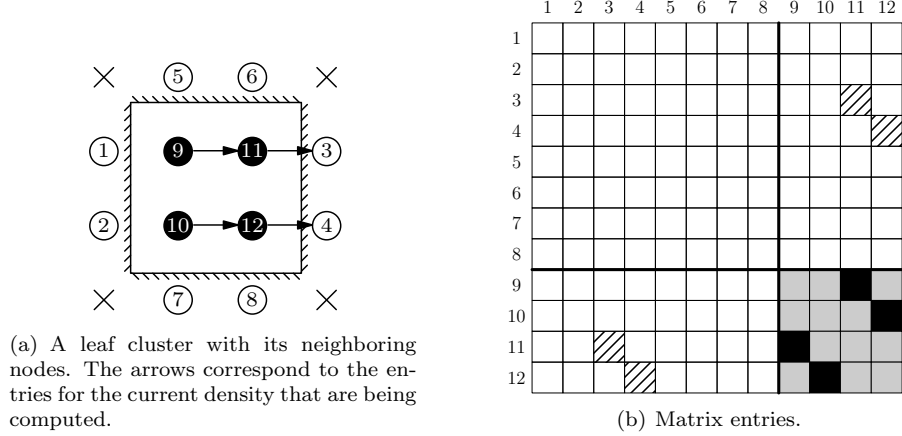


Figure 5: Last step of elimination. The entries in the shaded area are obtained through computing  $\mathbf{G}^r$ . The solid blocks and the patterned blocks are the off-diagonal entries for the current density. The solid blocks are obtained for free when we compute the diagonal entries of  $\mathbf{G}^r$ . The patterned blocks need to be computed separately.

Fig. 5 shows a small number of mesh nodes and their corresponding matrix entries for the computation of the diagonal entries  $\mathbf{G}^r$  and the current density. The entries of  $\mathbf{G}^r = \mathbf{A}^{-1}$  corresponding to the nodes in  $C$  are being computed with the following equation:

$$[\mathbf{A}^{-1}](C, C) = [\mathbf{A}(C, C) - \mathbf{A}(C, B_{\bar{C}})(\mathcal{U}_{\bar{C}})^{-1}\mathbf{A}(B_{\bar{C}}, C)]^{-1}. \quad (8)$$

The current density between nodes 9 and 11, and that between nodes 10 and 12 are also given by (8). To compute the current density between nodes 11 and 3 and that between nodes 12 and 4, perform one step of back substitution and we have

$$[\mathbf{A}^{-1}](B_{\bar{C}}, C) = -(\mathcal{U}_{\bar{C}})^{-1}\mathbf{A}(B_{\bar{C}}, C)[\mathbf{A}^{-1}](C, C) \quad (9)$$

and

$$[\mathbf{A}^{-1}](C, B_{\bar{C}}) = -[\mathbf{A}^{-1}](C, C)\mathbf{A}(C, B_{\bar{C}})(\mathcal{U}_{\bar{C}})^{-1}. \quad (10)$$

This can be generalized to nodes that are farther away.

## 4 Optimization of FIND

In our FIND algorithm, we achieved  $\mathcal{O}(N_x^2 N_y)$  computation complexity for a 2D mesh of size  $N_x \times N_y$ . Even though this complexity has been reduced by an order of magnitude compared to the state-of-the-art RGF method, the matrix inversion is still the most time consuming part in transport problem simulations. This chapter discusses how to further reduce the computational cost by using certain properties of the matrix  $\mathbf{A}$  such as its sparsity pattern.

In the FIND algorithm, the major operation is performing Gaussian eliminations. All such operations are of the form

$$\mathcal{U} = \mathbf{A}(\mathbf{B}, \mathbf{B}) - \mathbf{A}(\mathbf{B}, \mathbf{S})\mathbf{A}(\mathbf{S}, \mathbf{S})^{-1}\mathbf{A}(\mathbf{S}, \mathbf{B}) \quad (11)$$

for  $\mathbf{G}^r$  and

$$\mathcal{R} = \mathbf{\Sigma}(\mathbf{B}, \mathbf{B}) - \mathcal{L}\mathbf{\Sigma}(\mathbf{S}, \mathbf{B}) - \mathbf{\Sigma}(\mathbf{B}, \mathbf{S})\mathcal{L}^\dagger + \mathcal{L}\mathbf{\Sigma}(\mathbf{S}, \mathbf{S})\mathcal{L}^\dagger \quad (12)$$

for  $\mathbf{G}^<$ , where

$$\mathcal{L} = \mathbf{A}(\mathbf{B}, \mathbf{S})\mathbf{A}(\mathbf{S}, \mathbf{S})^{-1}. \quad (13)$$

These equations are copied from (2) and (7) with subscripts skipped for simplicity.<sup>2</sup> As a result, computing (11) and (12) efficiently becomes critical for our algorithm to achieve good overall performance.

Simple analysis [5] shows that the computation cost for (11) is

$$\frac{1}{3}s^3 + s^2b + sb^2 \quad (14)$$

and for (12) is

$$s^2b + 3sb^2, \quad (15)$$

where  $s$  and  $b$  are the size of sets  $\mathbf{S}$  and  $\mathbf{B}$ , respectively. These costs assume that all the matrices in (11) and (12) are general dense matrices. These matrices, however, are themselves sparse for a typical 2D mesh. In addition, due to the characteristics of the physical problem in many real applications, the matrices  $\mathbf{A}$  and  $\mathbf{\Sigma}$  often have special properties [21]. Such sparsities and properties will not change the order of cost, but may reduce the constant factor of the cost, thus achieving some measure of speed-up. With proper optimization, the FIND algorithm can exceed other algorithms on a much smaller mesh.

In this section, we first exploit the sparsity of the matrices in (2) and (7) to reduce the constant factor in the computation and the storage cost. We then consider the symmetry and positive definiteness of the given matrix  $\mathbf{A}$  for further performance improvement. Finally, we also apply these optimization techniques to  $\mathbf{G}^<$  and current density, when  $\mathbf{\Sigma}$  has similar properties.

## 4.1 Optimizations that depend on the sparsity of $\mathbf{A}$

Because of the local connectivity of the 2D mesh in our approach<sup>3</sup>, the matrices  $\mathbf{A}(\mathbf{B}, \mathbf{S})$ ,  $\mathbf{A}(\mathbf{S}, \mathbf{S})$ , and  $\mathbf{A}(\mathbf{S}, \mathbf{B})$  in (11) are not dense. Such sparsity will not reduce the storage cost since the matrix  $\mathcal{U}$  in (11) is dense and this is the major part of the storage cost. However, the computational cost can be significantly reduced. To clearly observe the sparsity and exploit it, it is convenient to consider these matrices in blocks.

### 4.1.1 Schematic description and analysis of the sparsity pattern

As shown earlier in Fig. 4, we eliminate the private inner nodes when we merge two child clusters in the tree into their parent cluster. In Figs. 6, we distinguish between the left and right clusters in the merge (compare with Fig. 4).

In Fig. 6, the three hollow circle nodes and the three hollow square nodes are private inner nodes of the parent cluster. They originate from the left child cluster and the right child cluster and are denoted as  $\mathbf{S}_L$  and  $\mathbf{S}_R$ , respectively. When we merge the two child clusters, these nodes will be eliminated. Similarly, the solid circle nodes and the solid square nodes are boundary nodes originated from the left and the right child clusters and are denoted as  $\mathbf{B}_L$  and  $\mathbf{B}_R$ , respectively. When we merge the two child clusters, these nodes will

<sup>2</sup>We use loose notations here since some of the entries of  $\mathbf{A}(\mathbf{S}, \mathbf{S})$  and  $\mathbf{\Sigma}(\mathbf{S}, \mathbf{S})$  have been modified by the Gaussian elimination compared to the original  $\mathbf{A}$  and  $\mathbf{\Sigma}$ . See Section 3.1 for details.

<sup>3</sup>The approach works for 3D mesh as well

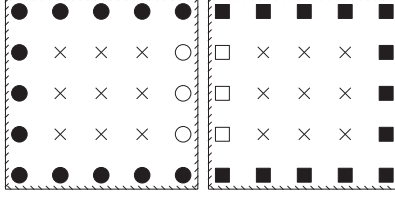


Figure 6: Two clusters merge into one larger cluster in the upward pass. The  $\times$  nodes have already been eliminated. The  $\circ$  and  $\square$  nodes remain to be eliminated. This figure is slightly different from Fig. 4 as we distinguish the nodes in the left and right clusters here.

be updated. The matrix blocks corresponding to the circle and square nodes can be written as

$$\begin{pmatrix} \mathbf{U}(\circ, \circ) & \mathbf{A}(\circ, \square) & \mathbf{U}(\circ, \bullet) & \mathbf{0} \\ \mathbf{A}(\square, \circ) & \mathbf{U}(\square, \square) & \mathbf{0} & \mathbf{U}(\square, \blacksquare) \\ \mathbf{U}(\bullet, \circ) & \mathbf{0} & \mathbf{U}(\bullet, \bullet) & \mathbf{A}(\bullet, \blacksquare) \\ \mathbf{0} & \mathbf{U}(\blacksquare, \square) & \mathbf{A}(\blacksquare, \bullet) & \mathbf{U}(\blacksquare, \blacksquare) \end{pmatrix}, \quad (16)$$

and the merge corresponds to the elimination of the first two columns of (16). If we follow the notation used in Section 2.2, then (16) corresponds to  $\mathbf{A}_k(\mathbf{S}_k \cup \mathbf{B}_k, \mathbf{S}_k \cup \mathbf{B}_k)^4$ , where cluster  $k$  has two child clusters  $i$  and  $j$ , and the circle and square nodes are given by:

- $\circ$ :  $\mathbf{S}_L = \mathbf{S}_k \cap \mathbf{B}_i$ , private inner nodes from the left cluster  $i$
- $\square$ :  $\mathbf{S}_R = \mathbf{S}_k \cap \mathbf{B}_j$ , private inner nodes from the right cluster  $j$
- $\bullet$ :  $\mathbf{B}_L = \mathbf{B}_k \cap \mathbf{B}_i$ , boundary nodes from the left cluster  $i$
- $\blacksquare$ :  $\mathbf{B}_R = \mathbf{B}_k \cap \mathbf{B}_j$ , boundary nodes from the right cluster  $j$

In (16) we use  $\mathbf{U}$  instead of  $\mathbf{A}$  for some blocks to emphasize that they are results from earlier eliminations while the other blocks come from the original matrix  $\mathbf{A}$ .<sup>5</sup> These  $\mathbf{U}$  blocks are typically dense, since after the elimination of the inner nodes, the remaining nodes become fully connected. In contrast, the  $\mathbf{A}$  blocks are typically sparse. For example, since each  $\circ$  node is connected with only one  $\square$  node in Fig. 6,  $\mathbf{A}(\circ, \square)$  and  $\mathbf{A}(\square, \circ)$  are both diagonal.  $\mathbf{A}(\bullet, \blacksquare)$  and  $\mathbf{A}(\blacksquare, \bullet)$  are almost all 0 except for a few entries, although such sparsity saves little cost because they are only involved in addition operations.

These properties always hold for the upward pass. They hold for the downward pass as well but with a few exceptions. These exceptions are illustrated by the patterned nodes in Fig. 7. Since the exceptions only occur at the corner nodes, we can ignore them in the computational and storage cost analysis.

<sup>4</sup>We use  $k$  instead of  $g$  here.

<sup>5</sup>We use loose notation here. The notations  $\mathbf{U}$  for some of the blocks (e.g.,  $\mathbf{U}(\bullet, \bullet)$ ) is incorrect since this is not the final  $\mathbf{U}$  matrix from the LU factorization, but rather an intermediate step in the method. This notation is closer to a computer code implementation. More precise notations however would reduce the legibility of the text.

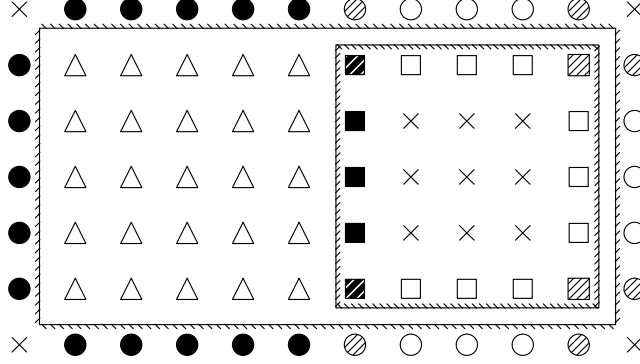


Figure 7: Notations are the same as in Fig. 6, with some nodes patterned. The  $\Delta$  nodes are not modified in this merging step. The patterned symbols correspond to nodes whose connectivity is different from Fig. 6. As a result,  $\mathbf{A}(\circ, \square)$  and  $\mathbf{A}(\square, \circ)$  are no longer strictly diagonal and  $\mathbf{A}(\circ, \blacksquare)$  is not exactly zero any more.

#### 4.1.2 Exploiting the sparsity using a block structure

We analyzed the computational cost using different formulas to calculate the inverse of a general  $2 \times 2$  block matrix. The following forms of the inverse are available:<sup>6</sup>

$$\begin{pmatrix} A & B \\ C & D \end{pmatrix}^{-1} = \begin{pmatrix} \tilde{A}^{-1} & -A^{-1}B\tilde{D}^{-1} \\ -D^{-1}C\tilde{A}^{-1} & \tilde{D}^{-1} \end{pmatrix} \quad (17a)$$

$$= \begin{pmatrix} A^{-1} + A^{-1}B\tilde{D}^{-1}CA^{-1} & -A^{-1}B\tilde{D}^{-1} \\ -\tilde{D}^{-1}CA^{-1} & \tilde{D}^{-1} \end{pmatrix} \quad (17b)$$

$$= \begin{pmatrix} A & B \\ 0 & \tilde{D} \end{pmatrix}^{-1} \begin{pmatrix} I & 0 \\ CA^{-1} & I \end{pmatrix}^{-1}, \quad (17c)$$

where  $\tilde{A} = A - BD^{-1}C$  and  $\tilde{D} = D - CA^{-1}B$  are the Schur complements of  $D$  and  $A$ , respectively. In (17a), the calculations for  $\tilde{A}^{-1}$  and  $\tilde{D}^{-1}$  are independent of each other and can be done in parallel, so we call this method *parallel inverse*. In (17b), we have to calculate  $\tilde{D}^{-1}$  first to calculate the other block of the inverse:  $A^{-1} + A^{-1}B\tilde{D}^{-1}CA^{-1}$ , so we call this method *sequential inverse*. In (17c), we perform block LU factorization first and then calculate the inverse, so we call this method *block LU inverse*.

Details of our derivation can be found in the appendix. Using our analysis of the sparsity pattern, the cost for each approach is shown in the table below:

Table 1: Summary of the optimization methods.

Method	Cost	Reduction in four cases <sup>7</sup>	Parallelism
parallel inverse	$\frac{8}{3}m^3 + 4m^2n + 4mn^2$	51.4, 52.6, 61.5, 60.1	good
sequential inverse	$\frac{4}{3}m^3 + 5m^2n + 4mn^2$	53.0, 54.0, 55.8, 55.7	little
block LU inverse	$\frac{4}{3}m^3 + 4m^2n + 5mn^2$	59.1, 57.9, 53.9, 54.3	some
naïve LU	$\frac{8}{3}m^3 + \frac{13}{2}m^2n + 4mn^2$	59.0, 62.5, 76.0, 74.4	little

Note that these methods are not exhaustive. There are many variations of these methods with different forms of  $\mathbf{A}(\mathbf{S}, \mathbf{S})^{-1}$ , different computation orders, and different common parts in the computation. Deter-

<sup>6</sup>We assume  $A$  and  $D$  to be nonsingular.

<sup>7</sup>The percentage of the cost given by (14).

mining which method is the best may depend on the size of  $S_L$ ,  $S_R$ ,  $B_L$ , and  $B_R$ , the exceptions in the downward pass (corner nodes), the flop rate, the cache miss rate, and the implementation complexity.

## 4.2 Optimization for symmetry and positive definiteness properties

In real problems,  $\mathbf{A}$  is often symmetric (or Hermitian if they are complex, which can be treated in a similar way) [21]. So it is worthwhile to consider special treatment for such matrices to reduce both computation cost and storage cost. Note that this reduction is independent of the optimizations based on the sparsity pattern in Section. 4.1.

If all the given matrices are symmetric, it is reasonable to expect the elimination results to be symmetric as well since our update rule (11) does not break matrix symmetry. This is shown in the following *property of symmetry preservation*:

**Property 1 (symmetry preservation)** *If  $\mathbf{A}$  is symmetric, then in (11),  $\mathcal{U}$ ,  $\mathbf{A}(\mathbf{B}, \mathbf{B})$ , and  $\mathbf{A}(\mathbf{S}, \mathbf{S})$  are all symmetric;  $\mathbf{A}(\mathbf{B}, \mathbf{S})$  and  $\mathbf{A}(\mathbf{S}, \mathbf{B})$  are transpose of each other.*

See A for a proof.

In addition,  $\mathbf{A}$  is often positive definite. This property is also preserved during the elimination process in our algorithm, as shown in the following *property of positive-definiteness preservation*:

**Property 2 (positive-definiteness preservation)** *If  $\mathbf{A}$  is symmetric and positive-definite, then the matrix  $\mathcal{U}$  in (11) is always positive-definite.*

See B for a proof. Using the symmetry preservation property and the positive definiteness preservation property, we can write the last term in (11) as

$$\mathbf{A}(\mathbf{B}, \mathbf{S})\mathbf{A}(\mathbf{S}, \mathbf{S})^{-1}\mathbf{A}(\mathbf{S}, \mathbf{B}) = (\mathcal{G}_S^{-1}\mathbf{A}(\mathbf{S}, \mathbf{B}))^T(\mathcal{G}_S^{-1}\mathbf{A}(\mathbf{S}, \mathbf{B})),$$

where  $\mathbf{A}(\mathbf{S}, \mathbf{S}) = \mathcal{G}_S\mathcal{G}_S^T$  is the Cholesky factorization of  $\mathbf{A}(\mathbf{S}, \mathbf{S})$ . The Cholesky factorization has cost  $\frac{1}{6}s^3$ . The solver has cost  $\frac{1}{2}s^2\mathbf{b}$ , and the final multiplication has cost  $\frac{1}{2}\mathbf{s}\mathbf{b}^2$ . The cost for (11) is then reduced by half from  $\frac{1}{3}s^3 + s^2\mathbf{b} + \mathbf{s}\mathbf{b}^2$  to  $\frac{1}{6}s^3 + \frac{1}{2}s^2\mathbf{b} + \frac{1}{2}\mathbf{s}\mathbf{b}^2$ .

Note that even if  $\mathbf{A}$  is not positive definite, by the symmetry preservation property alone, we can still write the last term of (11) as

$$\mathbf{A}(\mathbf{B}, \mathbf{S})\mathbf{A}(\mathbf{S}, \mathbf{S})^{-1}\mathbf{A}(\mathbf{S}, \mathbf{B}) = (\mathcal{L}_S^{-1}\mathbf{A}(\mathbf{S}, \mathbf{B}))^T\mathbf{D}_S^{-1}(\mathcal{L}_S^{-1}\mathbf{A}(\mathbf{S}, \mathbf{B})),$$

where  $\mathbf{A}(\mathbf{S}, \mathbf{S}) = \mathcal{L}_S\mathbf{D}_S\mathcal{L}_S^T$  is the LDL<sup>T</sup> factorization of  $\mathbf{A}(\mathbf{S}, \mathbf{S})$ .

Similarly, the computation cost is reduced by half. However, this method may be subject to large errors due to small pivots, since the pivots can only be selected from the diagonal entries [33]. The diagonal pivoting method [34, 35] can be used to solve such a problem, but it is computationally more expensive.

**Combining symmetry and sparsity** For symmetric and positive definite  $\mathbf{A}$ , we can take advantage of the sparsity pattern discussed in Section 4.1 as well. Consider the following block Cholesky factorization of  $\mathbf{A}(\mathbf{S}, \mathbf{S})$ :

$$\mathbf{A}(\mathbf{S}, \mathbf{S}) = \begin{pmatrix} \mathbf{A}_{11} & \mathbf{A}_{12} \\ \mathbf{A}_{12}^T & \mathbf{A}_{22} \end{pmatrix} = \begin{pmatrix} \mathcal{G}_1 & 0 \\ \mathbf{A}_{12}^T\mathcal{G}_1^{-T} & \widetilde{\mathcal{G}}_2 \end{pmatrix} \begin{pmatrix} \mathcal{G}_1^T & \mathcal{G}_1^{-1}\mathbf{A}_{12} \\ 0 & \widetilde{\mathcal{G}}_2^T \end{pmatrix} = \mathcal{G}_S\mathcal{G}_S^T, \quad (18)$$

where  $\mathbf{A}_{11} = \mathcal{G}_1\mathcal{G}_1^T$ ,  $\widetilde{\mathbf{A}}_{22} = \mathbf{A}_{22} - \mathbf{A}_{12}^T\mathbf{A}_{11}^{-1}\mathbf{A}_{12}$ , and  $\widetilde{\mathbf{A}}_{22} = \widetilde{\mathcal{G}}_2\widetilde{\mathcal{G}}_2^T$ . Now, we have

$$\begin{aligned} \mathcal{G}_S^{-1}\mathbf{A}(\mathbf{S}, \mathbf{B}) &= \begin{pmatrix} \mathcal{G}_1 & 0 \\ \mathbf{A}_{12}^T\mathcal{G}_1^{-T} & \widetilde{\mathcal{G}}_2 \end{pmatrix} \begin{pmatrix} \mathbf{A}_i(\mathbf{S}_k \cap \mathbf{B}_i, \mathbf{B}_k \cap \mathbf{B}_i) & 0 \\ 0 & \mathbf{A}_j(\mathbf{S}_k \cap \mathbf{B}_j, \mathbf{B}_k \cap \mathbf{B}_j) \end{pmatrix} \\ &= \begin{pmatrix} \mathcal{G}_1^{-1}\mathbf{A}(\mathbf{S}_L, \mathbf{B}_L) & 0 \\ -\widetilde{\mathcal{G}}_2^{-1}\mathbf{A}_{12}^T\mathcal{G}_1^{-T}\mathcal{G}_1^{-1}\mathbf{A}(\mathbf{S}_L, \mathbf{B}_L) & \widetilde{\mathcal{G}}_2^{-1}\mathbf{A}(\mathbf{S}_R, \mathbf{B}_R) \end{pmatrix}. \end{aligned} \quad (19)$$



and

$$\mathbf{A}(\mathbf{B}, \mathbf{S})\mathbf{A}(\mathbf{S}, \mathbf{S})^{-1}\mathbf{A}(\mathbf{S}, \mathbf{B}) = (\mathcal{G}_5^{-1}\mathbf{A}(\mathbf{S}, \mathbf{B}))^T(\mathcal{G}_5^{-1}\mathbf{A}(\mathbf{S}, \mathbf{B})). \quad (20)$$

With these different optimizations, the total cost ends up being  $\frac{2}{3}m^3 + 2m^2n + \frac{5}{2}mn^2$ . Compared to the original cost with a block structure, the cost is reduced by more than half when  $m = n$ . The cost with both optimizations, for sparsity and symmetry, is 25% of the original cost when the condition  $m \approx \frac{\sqrt{3}}{2}n$  is satisfied.

**Storage cost reduction** In addition to the computation cost reduction, the storage cost can also be reduced for symmetric  $\mathbf{A}$ . Since the storage cost is mainly for  $\mathcal{U}$ , which is always symmetric, the storage cost is reduced by half. Another part of the storage cost comes from the temporary space needed for (11), which can also be reduced by half. Such space is needed for the top level update in the cluster tree. It is about the same as the cost for  $\mathcal{U}$  but we do not have to keep it. So for a typical cluster tree with ten or more levels, this part is not important. When the mesh size is small with a short cluster tree, this part and its reduction may be important.

### 4.3 Optimization for computing $\mathbf{G}^<$ and current density

We can also reduce the cost for computing  $\mathbf{G}^<$  by optimizing the procedure for (12):

$$\mathcal{R} = \Sigma(\mathbf{B}, \mathbf{B}) - \mathcal{L}\Sigma(\mathbf{S}, \mathbf{B}) - \Sigma(\mathbf{B}, \mathbf{S})\mathcal{L}^\dagger + \mathcal{L}\Sigma(\mathbf{S}, \mathbf{S})\mathcal{L}^\dagger \quad (21)$$

We now consider optimizations that use the sparsity pattern of  $\mathbf{A}$  and  $\Sigma$ , and separately the symmetry of  $\mathbf{A}$  and  $\Sigma$ . Those optimizations can be combined but this will not be presented in this paper.

#### 4.3.1 $\mathbf{G}^<$ sparsity

Since  $\Sigma(\mathbf{S}, \mathbf{B})$  and  $\Sigma(\mathbf{B}, \mathbf{S})$  are block diagonal, the cost for the second and the third term in (21) is reduced by half. Similar to the structure of  $\mathbf{A}(\mathbf{S}, \mathbf{S})$  in (11), the blocks  $\Sigma(\mathbf{S}_k \cap \mathbf{B}_i, \mathbf{S}_k \cap \mathbf{B}_j)$  and  $\Sigma(\mathbf{S}_k \cap \mathbf{B}_j, \mathbf{S}_k \cap \mathbf{B}_i)$  in  $\Sigma(\mathbf{S}_k, \mathbf{S}_k)$  are diagonal. Consequently, the computational cost of operating with these blocks will be ignored since it is negligible. The cost for the fourth term  $\mathcal{L}^{-1}\Sigma(\mathbf{S}, \mathbf{S})\mathcal{L}^{-\dagger}$  in (21) is then reduced to  $\frac{1}{2}s^2\mathbf{b} + s\mathbf{b}^2$  (or  $s^2\mathbf{b} + \frac{1}{2}s\mathbf{b}^2$ , depending on the order of computation). So the total cost for (21) becomes  $\frac{1}{2}s^2\mathbf{b} + 2s\mathbf{b}^2$  (or  $s\mathbf{b} + \frac{3}{2}s\mathbf{b}^2$ ). Compared with the cost without optimization for sparsity, it is reduced by 37.5% when  $s = \mathbf{b}$ .

In addition,  $\Sigma$  is often diagonal or 3-diagonal in real problems. As a result,  $\Sigma(\mathbf{S}_k \cap \mathbf{B}_i, \mathbf{S}_k \cap \mathbf{B}_j)$  and  $\Sigma(\mathbf{S}_k \cap \mathbf{B}_j, \mathbf{S}_k \cap \mathbf{B}_i)$  become zero and  $\Sigma_k(\mathbf{S}_k, \mathbf{S}_k)$  becomes block diagonal. This can lead to further reduction.

#### 4.3.2 $\mathbf{G}^<$ symmetry

For symmetric  $\Sigma$ , we have a property of symmetry and positive definiteness preservation for  $\Sigma_{g^+}(\mathbf{B}_g, \mathbf{B}_g)$ ,  $\Sigma_g(\mathbf{B}_g, \mathbf{B}_g)$ , and  $\Sigma_g(\mathbf{S}_g, \mathbf{S}_g)$ . With such symmetry, we can perform a Cholesky factorization on  $\Sigma(\mathbf{S}, \mathbf{S}) = \mathcal{K}_5\mathcal{K}_5^T$ . The total cost for (7) is reduced to  $\frac{1}{6}s^3 + s^2\mathbf{b} + \frac{3}{2}s\mathbf{b}^2$ . Compared to the cost of computation without exploiting the symmetry ( $s^2\mathbf{b} + 3s\mathbf{b}^2$ ), the cost is reduced by approximately 33% when  $s = \mathbf{b}$ .

#### 4.3.3 Current density

We can also exploit the sparsity when computing the current density, but it cannot improve much since there is not as much sparsity in (8)–(10) as in (11). This can be seen in Fig. 8.

However, we can significantly reduce the cost with another approach. In this approach, we still compute the entries of  $\mathbf{G}^r$  for every leaf cluster, but compute the current density only for half of the leaf clusters indicated by the solid nodes in Fig. 9(a). This approach is still based on (8)–(10), but in addition to computing the current density for nodes 9–12, we also compute the current density for nodes 1 and 2, which incurs no extra cost. Therefore, it reduces the cost for the current density by half.

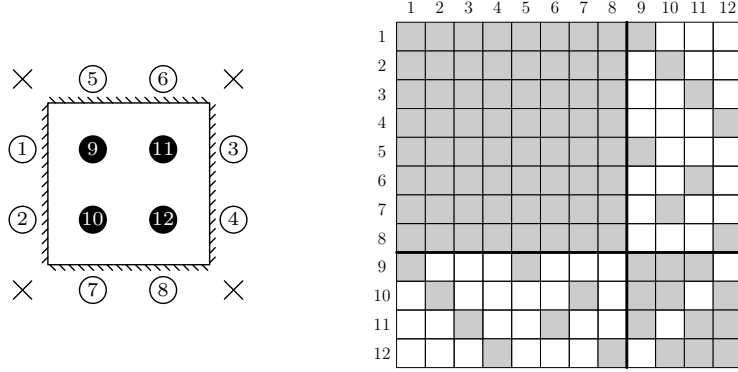


Figure 8: Sparsity of the matrices before the last step of elimination. Shaded blocks are non-zero entries and blank blocks are zero entries.

Moreover, if for the chosen leaf clusters, we compute not only the off-diagonal entries for the current density, but also the diagonal entries for nodes 5–12, then we can completely avoid the last step of elimination and the computation thereafter for the other half of the leaf clusters in the final stage. Detailed analysis shows that computing both the diagonal entries of  $\mathbf{G}^r$  and the current density with this approach is in fact even less costly than computing only the diagonal entries of  $\mathbf{G}^r$  without this approach. Fig. 9 shows how we choose the leaf clusters to cover the desired diagonal and off-diagonal entries in  $\mathbf{G}^r$ . Note that this approach (even though more efficient) was not implemented in our numerical benchmarks.

We can also optimize (8)–(10) by similar techniques used in Section 4.2 to reduce the cost for symmetric  $\mathbf{A}$  and  $\Sigma$ . In (8),

$$\mathbf{A}(C, C) - \mathbf{A}(C, B_{\bar{C}})(\mathcal{U}_{\bar{C}})^{-1}\mathbf{A}(B_{\bar{C}}, C)$$

is of the same form as (11) so the cost is reduced by half. The cost of computing its inverse is also reduced by half when it is symmetric. Eqs. (9) and (10) are transpose of each other so we only need to compute one of them. As a result, the cost for computing the current density is reduced by half using symmetry.

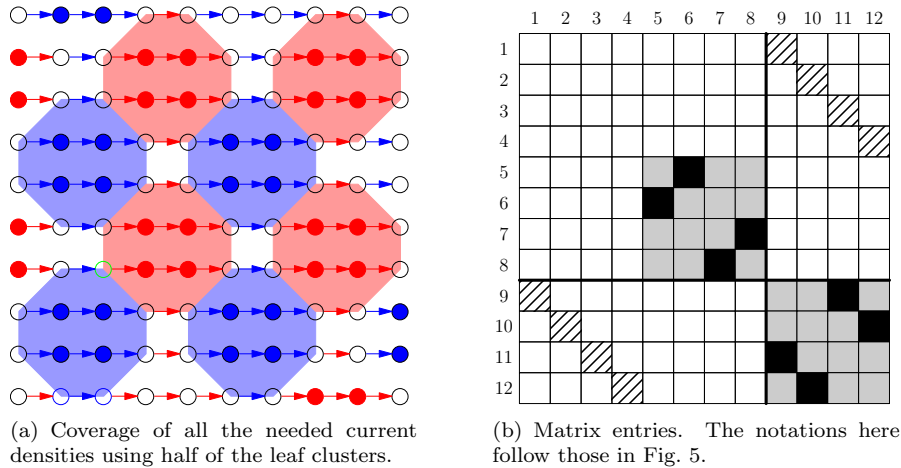


Figure 9: Choice of leaf clusters and the corresponding matrix with desired entries marked. Each needed cluster consists of four solid nodes. The circle nodes are “skipped.” Arrows correspond to the current densities. If we compute the entries in the shaded area and in the patterned blocks, then all the desired entries will be covered. See Fig. 8 for the node numbering.

## 4.4 Nodes on the physical boundary of the device

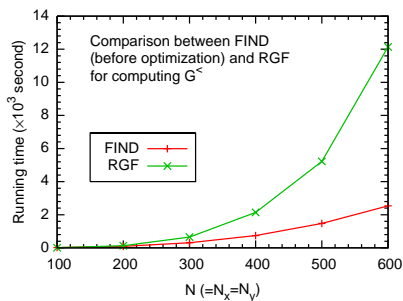
Some of the nodes on the physical boundary of the device have a different connectivity. For example, a typical node in a 5 point stencil is connected to 4 neighbors. A node on the physical boundary of the device may be connected to only 3 neighbors. This reduces the computational cost of our method since those nodes can be eliminated early in the scheme leading to overall smaller boundary sets for some of the clusters. This has a small effect for leaf clusters (i.e., small clusters) but leads to a significant reduction in the computational cost near the root of the tree when we have few very large clusters. With such effect taken into consideration, the total cost of the algorithm is approximately  $457N^3$  (see the appendix). As a comparison, the cost using RGF with symmetry taken into consideration is  $3.5N^4$ . Since the cross-point of the two cost curves is at  $N$  equal to the ratio between the constant factors in the two methods, it is expected to happen at  $N \sim 130$ . This is consistent with what we observed in our simulations.

*Section Summary.* The optimization for sparsity leads to 40% cost reduction and that for symmetry leads to 50% cost reduction. This results in a 70% cost reduction. In other words, the new cost is about  $\mathbf{1/3}$  of the original cost. This is reflected in the cross-point of the performance curves using these two methods. Originally, the cross-point was around  $N \sim 130$ , but now it can be as low as  $N = 40$ . This shows the performance improvement resulting from our optimizations. The optimization for sparsity does not reduce the memory cost. The optimization for symmetry does reduce it (approximately by half).

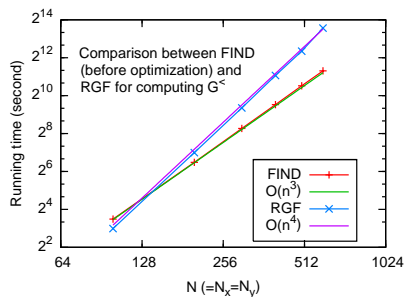
## 5 Numerical Results

### 5.1 Extension

In the following two figures, Fig. 10(a) gives the running time for computing  $\mathbf{G}^<$  based on the extension of FIND as described in Section 3 and the comparison with RGF. Fig. 10(b) shows the same data in log-log scale to see more clearly the asymptotic behavior of these two methods. All the running times in these two figures are based on the extension of FIND before the optimizations discussed in Section 4.



(a) Running time comparison



(b) Running time in log-log scale to see the asymptotic behavior

Figure 10: Comparison of running time based on FIND extension (before optimization) and RGF for computing  $\mathbf{G}^<$

### 5.2 Optimization

Fig. 11(a) shows the computation cost reduction for clusters of different sizes during the upward pass, after optimization for sparsity. As indicated in Section 4.1, the improvements are different for two types of merge: i) two  $(a \times a)$ -clusters  $\Rightarrow$  one  $(a \times 2a)$ -cluster; ii) two  $(2a \times a)$ -clusters  $\Rightarrow$  one  $(2a \times 2a)$ -cluster, so they are shown separately in the figure. The reduction for small clusters is not as significant. This is because the

second order contributions to the cost (e.g.,  $\mathcal{O}(m^2)$ ) was ignored in our analysis but is significant for small clusters.

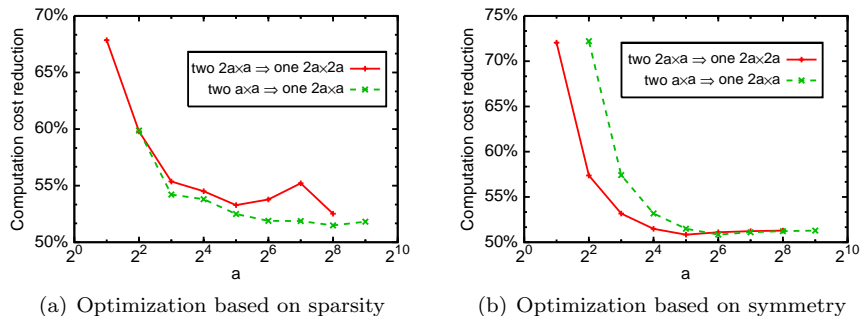


Figure 11: Comparison between RGF and FIND after optimization

Fig.11(b) shows the computation cost reduction after optimization for symmetry. Similar to the Fig. 11(a), we show the reduction when merging clusters at each level in the basic cluster tree. We can see that the cost is reduced almost by half for clusters larger than  $32 \times 32$ . The smaller reduction for small clusters is mainly

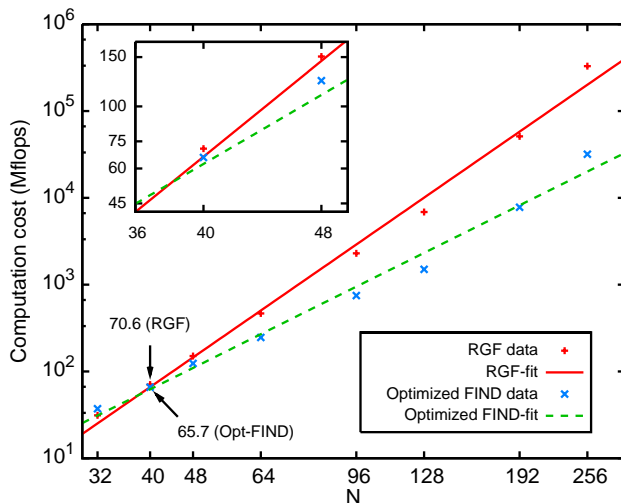


Figure 12: Comparison with RGF to show the change of cross-point

due to the fact that the Cholesky factorization does not provide savings by a factor of 2 for these clusters. Although the reduction in cost is smaller for small clusters using either optimizations, these clusters do not play a significant role for a mesh larger than  $32 \times 32$  since the top levels of the tree in Fig. 2(a) dominate the computation cost.

Fig. 12 compares the computation cost of RGF and optimized FIND on a Hermitian and positive-definite matrix  $\mathbf{A}$  and shows the overall effect of the optimization for sparsity and symmetry. The simulations were performed on a square mesh of size  $N \times N$ . The cross-point is around  $40 \times 40$  according to the two fitted lines. We confirmed this by adding a simulation at that point.

## 6 Conclusion and discussion

We have presented an extension of the method described in [5] to the calculation on  $\mathbf{G}^<$  and the current density in NEGF models of nano-transistors. This extension is essential to apply the methods in [5] to real engineering problems. This extension assumes that  $\Sigma$  has a sparsity pattern similar to  $\mathbf{A}$ . It is based on a nested dissection of the mesh and uses a form of Gaussian elimination. In the family of direct methods that provide exact solutions (vs approximate methods), it can be proved that the scaling of the computational cost with problem size using nested dissection is optimal.

We considered the case of a typical finite-difference scheme for a two dimensional device. The sparsity pattern associated with the stencil allows special optimizations, which can reduce the computational cost by a factor of approximately 2. These optimizations are generally applicable to other types of finite-difference stencils, even though this extension was not discussed here. When  $\Sigma$  is sparser than  $\mathbf{A}$ , for example if it is a diagonal matrix, further cost reductions are possible.

We also presented optimizations for the cases where  $\mathbf{A}$  is symmetric. In this case, the computational cost of many operations can be reduced using Cholesky type factorization. We also proved results regarding properties of positive definiteness for matrices arising in the process, for example  $\mathcal{U}$ . Those optimization techniques were derived for computing both  $\mathbf{G}$  and  $\mathbf{G}^<$ .

We described a simple approach to reduce the cost of computing the current, which uses an octagonal tiling of the mesh. This allows reducing the number of leaf clusters that are computed while yielding all the off-diagonal entries that are needed.

Finally, regarding the nodes on the physical boundary of the device, we calculated their effect on the computational cost. The cost associated with clusters that share nodes with the physical boundary of the device is typically lower since the size of the boundary set of the cluster is smaller. Consequently, this reduces significantly the computational cost of operating on the clusters near the top of the tree.

Numerical results confirm the computational cost analysis and show the speed-up that can be expected from applying these methods to real-life applications.

We have not discussed the role that certain classes of fast methods like multigrid algorithms can play for our problem. Multigrid algorithms have been used successfully to solve a wide range of linear systems  $\mathbf{A}x = b$  in linear time [36, 37]. In the area of semiconductor process and device simulation, multigrid has been applied, for example, to the solution of various partial differential equations, including Lamé equations (linear elasticity), reaction-diffusion (-convection) and drift-diffusion (-convection-reaction) systems [36]. In the NEGF area, multigrid has been used in the solution of the Kohn-Sham equations (specifically the associated generalized eigenvalue problem) [38, 39, 40, 41]. The computational cost of multigrid when solving a linear system is lower than the FIND algorithm. However, it is not known whether adapting multigrid from solving a linear system of equations  $\mathbf{A}x = b$  to computing in linear time the diagonal of  $\mathbf{G}^r = \mathbf{A}^{-1}$  and  $\mathbf{G}^r \Sigma [\mathbf{G}^r]^\dagger$  is possible.

## ACKNOWLEDGEMENT

We thank the Stanford School of Engineering, the Institute for Computational and Mathematical Engineering, and U.S. Army grant W911NF-07-2-0027 from the Army High Performance Computing Research Center for Agility, Survivability and Informatics at Stanford, for their support.

In the appendix we provide additional technical results that were used in the main body of this paper.

## A Symmetry preservation

*Proof:* This property holds for all the leaf clusters by the symmetry of the original matrix  $\mathbf{A}$ . For any node in the cluster tree, if the property holds for its two child clusters  $i$  and  $j$ , then the property holds for their

parent node  $k$  as well because the blocks of  $\mathbf{A}$  in (11) are given by

$$\mathbf{A}_k(\mathbf{B}_k, \mathbf{B}_k) = \begin{pmatrix} \mathbf{A}_i(\mathbf{B}_k \cap \mathbf{B}_i, \mathbf{B}_k \cap \mathbf{B}_i) & \mathbf{A}(\mathbf{B}_k \cap \mathbf{B}_i, \mathbf{B}_k \cap \mathbf{B}_j) \\ \mathbf{A}(\mathbf{B}_k \cap \mathbf{B}_j, \mathbf{B}_k \cap \mathbf{B}_i) & \mathbf{A}_j(\mathbf{B}_k \cap \mathbf{B}_j, \mathbf{B}_k \cap \mathbf{B}_j) \end{pmatrix}, \quad (22a)$$

$$\mathbf{A}_k(\mathbf{S}_k, \mathbf{S}_k) = \begin{pmatrix} \mathbf{A}_i(\mathbf{S}_k \cap \mathbf{B}_i, \mathbf{S}_k \cap \mathbf{B}_i) & \mathbf{A}(\mathbf{S}_k \cap \mathbf{B}_i, \mathbf{S}_k \cap \mathbf{B}_j) \\ \mathbf{A}(\mathbf{S}_k \cap \mathbf{B}_j, \mathbf{S}_k \cap \mathbf{B}_i) & \mathbf{A}_j(\mathbf{S}_k \cap \mathbf{B}_j, \mathbf{S}_k \cap \mathbf{B}_j) \end{pmatrix}, \quad (22b)$$

$$\mathbf{A}_k(\mathbf{B}_k, \mathbf{S}_k) = \begin{pmatrix} \mathbf{A}_i(\mathbf{B}_k \cap \mathbf{B}_i, \mathbf{S}_k \cap \mathbf{B}_i) & \mathbf{0} \\ \mathbf{0} & \mathbf{A}_j(\mathbf{B}_k \cap \mathbf{B}_j, \mathbf{S}_k \cap \mathbf{B}_j) \end{pmatrix}, \quad (22c)$$

$$\mathbf{A}_k(\mathbf{S}_k, \mathbf{B}_k) = \begin{pmatrix} \mathbf{A}_i(\mathbf{S}_k \cap \mathbf{B}_i, \mathbf{B}_k \cap \mathbf{B}_i) & \mathbf{0} \\ \mathbf{0} & \mathbf{A}_j(\mathbf{S}_k \cap \mathbf{B}_j, \mathbf{B}_k \cap \mathbf{B}_j) \end{pmatrix}. \quad (22d)$$

□

## B Positive-definiteness preservation

**Proof:** Write  $n \times n$  symmetric positive definite matrix  $\mathbf{A}$  as  $\begin{pmatrix} a_{11} & z^T \\ z & \bar{\mathbf{A}}_{11} \end{pmatrix}$  and let  $\tilde{\mathbf{A}}_{11} \stackrel{def}{=} \bar{\mathbf{A}}_{11} - zz^T/a_{11}$  be the Schur complement of  $a_{11}$ . Let  $\mathbf{A}^{(0)} \stackrel{def}{=} \mathbf{A}$ ,  $\mathbf{A}^{(1)} \stackrel{def}{=} \tilde{\mathbf{A}}_{11}^{(0)}$ ,  $\dots$ ,  $\mathbf{A}^{(n-1)} \stackrel{def}{=} \tilde{\mathbf{A}}_{11}^{(n-2)}$ . Note that since  $\mathbf{A}$  is positive definite,  $\mathbf{A}_{11}^{(i)} \neq 0$  and  $\tilde{\mathbf{A}}^{(i+1)}$  is well defined for all  $i = 0, \dots, n-2$ . By definition,  $\tilde{\mathbf{A}}^{(i+1)}$  are also all symmetric.

Now, we will show that  $\mathbf{A}^{(1)}, \dots, \mathbf{A}^{(n-1)}$  are all positive definite. Given any  $(n-1) \times 1$  matrix  $y \neq 0$ , let  $x = \begin{pmatrix} -z^T y/a_{11} \\ y \end{pmatrix} \neq 0$ . Since  $\mathbf{A}$  is symmetric positive definite, we have

$$\begin{aligned} 0 &< x^T \mathbf{A} x \\ &= \begin{pmatrix} -z^T y/a_{11} & y^T \end{pmatrix} \begin{pmatrix} a_{11} & z^T \\ z & \bar{\mathbf{A}}_{11} \end{pmatrix} \begin{pmatrix} -z^T y/a_{11} \\ y \end{pmatrix} \\ &= \begin{pmatrix} 0 & -y^T z z^T/a_{11} + y^T \bar{\mathbf{A}}_{11} \end{pmatrix} \begin{pmatrix} -z^T y/a_{11} \\ y \end{pmatrix} \\ &= -y^T z z^T y/a_{11} + y^T \bar{\mathbf{A}}_{11} y \\ &= y^T (\bar{\mathbf{A}}_{11} - z z^T/a_{11}) y \\ &= y^T \tilde{\mathbf{A}}_{11} y. \end{aligned}$$

As a result,  $\mathbf{A}^{(1)}$  is positive definite as well. Repeat this process to show that  $\mathbf{A}^{(2)}, \dots, \mathbf{A}^{(n-1)}$  are all positive definite.

Since any principal submatrix of a positive definite matrix is also positive definite [33], every  $\mathbf{A}(\mathbf{S}_k, \mathbf{S}_k)$  in (2) is also positive definite. □

## C Optimizations that use the sparsity of $\mathbf{A}$

The sparsity pattern was described in the main body of the paper. In this section, based on this sparsity pattern and different ways to calculate the inverse of a matrix, we reduce the number of floating point operations.

Recall that we need to calculate the term:

$$\mathbf{A}(\mathbf{B}, \mathbf{S}) \mathbf{A}(\mathbf{S}, \mathbf{S})^{-1} \mathbf{A}(\mathbf{S}, \mathbf{B})$$

which is part of the update of  $\mathcal{U}$ :

$$\mathcal{U} = \mathbf{A}(\mathbf{B}, \mathbf{B}) - \mathbf{A}(\mathbf{B}, \mathbf{S}) \mathbf{A}(\mathbf{S}, \mathbf{S})^{-1} \mathbf{A}(\mathbf{S}, \mathbf{B})$$

For notational simplicity, in this section, we write  $\mathbf{A}(\mathbf{S}, \mathbf{S})$  as a block matrix:

$$\begin{pmatrix} A & B \\ C & D \end{pmatrix} = \begin{pmatrix} \mathbf{A}(\mathbf{S}_L, \mathbf{S}_L) & \mathbf{A}(\mathbf{S}_L, \mathbf{S}_R) \\ \mathbf{A}(\mathbf{S}_R, \mathbf{S}_L) & \mathbf{A}(\mathbf{S}_R, \mathbf{S}_R) \end{pmatrix};$$

write  $\mathbf{A}(\mathbf{S}, \mathbf{B})$  as

$$\begin{pmatrix} W & X \\ Y & Z \end{pmatrix} = \begin{pmatrix} \mathbf{A}(\mathbf{S}_L, \mathbf{B}_L) & \mathbf{A}(\mathbf{S}_L, \mathbf{B}_R) \\ \mathbf{A}(\mathbf{S}_R, \mathbf{B}_L) & \mathbf{A}(\mathbf{S}_R, \mathbf{B}_R) \end{pmatrix};$$

and write  $\mathbf{A}(\mathbf{B}, \mathbf{S})$  as

$$\begin{pmatrix} P & Q \\ R & S \end{pmatrix} = \begin{pmatrix} \mathbf{A}(\mathbf{B}_L, \mathbf{S}_L) & \mathbf{A}(\mathbf{B}_L, \mathbf{S}_R) \\ \mathbf{A}(\mathbf{B}_R, \mathbf{S}_L) & \mathbf{A}(\mathbf{B}_R, \mathbf{S}_R) \end{pmatrix}.$$

Since a multiplication is much more expensive than an addition, we ignore the addition with  $\mathbf{A}(\mathbf{B}, \mathbf{B})$ .

Before proceeding to the main analysis, we list some facts about the computational cost of various basic matrix computations. We indicate the cost of various operations (shown with  $\Rightarrow$ ) involving the  $n \times n$  full matrices  $A$  and  $B$  (only multiplications are counted):

$$\begin{aligned} A &\Rightarrow LU : n^3/3 \\ L &\Rightarrow L^{-1} : n^3/6 \\ L, B &\Rightarrow L^{-1}B : n^3/2 \\ U, L^{-1}B &\Rightarrow A^{-1}B : n^3/2 \end{aligned}$$

Adding them together, computing  $A^{-1}$  requires  $n^3$  and computing  $A^{-1}B$  requires  $\frac{4}{3}n^3$ . The order of computation is often important, e.g., if we compute  $A^{-1}B = (U^{-1}L^{-1})B$ , then the cost is  $(n^3 + n^3) = 2n^3$ , whereas computing  $U^{-1}(L^{-1}B)$  only requires  $\frac{4}{3}n^3$ .

We will consider different block forms for the inverse:<sup>8</sup>

$$\begin{aligned} \begin{pmatrix} A & B \\ C & D \end{pmatrix}^{-1} &= \begin{pmatrix} \tilde{A}^{-1} & -A^{-1}B\tilde{D}^{-1} \\ -D^{-1}C\tilde{A}^{-1} & \tilde{D}^{-1} \end{pmatrix} \\ &= \begin{pmatrix} A^{-1} + A^{-1}B\tilde{D}^{-1}CA^{-1} & -A^{-1}B\tilde{D}^{-1} \\ -\tilde{D}^{-1}CA^{-1} & \tilde{D}^{-1} \end{pmatrix} \\ &= \begin{pmatrix} A & B \\ 0 & \tilde{D} \end{pmatrix}^{-1} \begin{pmatrix} I & 0 \\ CA^{-1} & I \end{pmatrix}^{-1} \end{aligned}$$

See (17a), (17b), and (17c). In (17a), the calculations for  $\tilde{A}^{-1}$  and  $\tilde{D}^{-1}$  are independent of each other and can be done in parallel, so we call this method *parallel inverse*. In (17b), we have to calculate  $\tilde{D}^{-1}$  first to calculate the other block of the inverse:  $A^{-1} + A^{-1}B\tilde{D}^{-1}CA^{-1}$ , so we call this method *sequential inverse*. In (17c), we perform block LU factorization first and then calculate the inverse, so we call this method *block LU inverse*.

The first method is based on (17a), the parallel inverse of the block matrix. It computes  $\mathbf{A}(\mathbf{S}, \mathbf{S})^{-1}$  through the Schur complement of the two diagonal blocks of  $\mathbf{A}(\mathbf{S}, \mathbf{S})$ . We multiply (17a) by  $\mathbf{A}(\mathbf{S}, \mathbf{B})$  on the right. The result of this multiplication is a  $2 \times 2$  block matrix, whose blocks are shown in Table 2. The calculation of each block requires a set of operations listed in the *Operations* columns. The details of how to perform those operations in order to minimize the computational cost are given in Table 3.

Table 3 gives the cost of each operation with different assumptions for the sparsity pattern of  $X$  and  $Y$ . The last column indicates the dependency between these operations, as some of the operations depend on the results of previous operations.

In this table and the tables below, to show dependence, the operations are listed in the order of computation. The size of  $A$ ,  $B$ ,  $C$ , and  $D$  is  $m \times m$ ; the size of  $W$ ,  $X$ ,  $Y$ , and  $Z$  is  $m \times n$ . The different operations are labeled using a number inside a circle. This notation was also used in Table 2.

<sup>8</sup>We assume  $A$  and  $D$  to be nonsingular.

Table 2: Matrix blocks and their corresponding operations

<i>Block</i>	<i>Expression</i>	<i>Operations</i>
(1, 1)	$\tilde{A}^{-1}W - A^{-1}B\tilde{D}^{-1}Y$	⑤ ⑫
(1, 2)	$\tilde{A}^{-1}X - A^{-1}B\tilde{D}^{-1}Z$	⑨ ⑧
(2, 1)	$-D^{-1}C\tilde{A}^{-1}W + \tilde{D}^{-1}Y$	⑦ ⑩
(2, 2)	$D^{-1}C\tilde{A}^{-1}X + \tilde{D}^{-1}Z$	⑪ ⑥

Table 3: The cost of operations and their dependence in the first method. The costs are in flops. The size of  $A, B, C$ , and  $D$  is  $m \times m$ ; the size of  $W, X, Y$ , and  $Z$  is  $m \times n$ .

<i>Operations</i>	<i>Type of matrix blocks</i>			<i>Dependency</i>
	all full	X, Y = 0	X, Y = 0; B, C = diag	
① $D \setminus C$	$4m^3/3$	$4m^3/3$	$m^3$	n/a
② $A \setminus B$	$4m^3/3$	$4m^3/3$	$m^3$	n/a
③ $\tilde{A} = A - BD^{-1}C$	$m^3$	$m^3$	0	①
④ $\tilde{D} = D - CA^{-1}B$	$m^3$	$m^3$	0	②
⑤ $\tilde{A} \setminus W$	$\frac{m^3}{3} + m^2n$	$\frac{m^3}{3} + m^2n$	$\frac{m^3}{3} + m^2n$	③
⑥ $\tilde{D} \setminus Z$	$\frac{m^3}{3} + m^2n$	$\frac{m^3}{3} + m^2n$	$\frac{m^3}{3} + m^2n$	④
⑦ $-D^{-1}C\tilde{A}^{-1}W$	$m^2n$	$m^2n$	$m^2n$	① ⑤
⑧ $-A^{-1}B\tilde{D}^{-1}Z$	$m^2n$	$m^2n$	$m^2n$	② ⑥
⑨ $\tilde{A}^{-1}X$	$m^2n$	0	0	⑤
⑩ $\tilde{D}^{-1}Y$	$m^2n$	0	0	⑥
⑪ $-D^{-1}C\tilde{A}^{-1}X$	$m^2n$	0	0	① ⑨
⑫ $-A^{-1}B\tilde{D}^{-1}Y$	$m^2n$	0	0	② ⑩
<b>Total</b>	$\frac{16m^3}{3} + 8m^2n$	$\frac{16m^3}{3} + 4m^2n$	$\frac{8m^3}{3} + 4m^2n$	n/a

Since the clusters are typically equally split, we can let  $m = |S_L| = |S_R| = |S|/2$  and  $n = |B_L| = |B_R| = |B|/2$ . Then, the size of matrices  $A, B, C$ , and  $D$  is  $m \times m$ ; the size of matrices  $W, X, Y$ , and  $Z$  is  $m \times n$ , and the size of matrices  $P, Q, R$ , and  $S$  is  $m \times n$ . For example, for a merge from two  $(a \times a)$ -clusters to one  $(a \times 2a)$ -cluster, we have  $m = a$  and  $n = 3a$ .

Table 3 gives the cost of computing  $\mathbf{A}(S, S)^{-1}\mathbf{A}(S, B)$  in (11). Consider now the multiplication by  $\mathbf{A}(B, S)$  from the left: it requires  $4m^2n$  operations. The total computation cost for (11) with the above optimization is therefore  $\frac{8}{3}m^3 + 4m^2n + 4mn^2$ . In contrast, the cost without optimization is  $8mn^2 + 8m^2n + \frac{8}{3}m^3$  since  $s = 2m$  and  $b = 2n$ .

Taking two upward cases as examples,  $(m, n) = (a, 3a)$  and  $(m, n) = (2a, 4a)$ , the reduction is:

$$\frac{296}{3}a^3 \rightarrow \frac{152}{3}a^3 \quad \text{and} \quad \frac{1216}{3}a^3 \rightarrow \frac{640}{3}a^3.$$

The cost with optimization lies somewhere between 51% to 53% of the original cost. Similarly, for the downward pass, in the two typical cases  $(m, n) = (3a, 2a)$  and  $(m, n) = (4a, 3a)$ , we have the reduction

$$312a^3 \rightarrow 192a^3 \text{ (62\%)} \quad \text{and} \quad \frac{2528}{3} \rightarrow \frac{1520}{3}a^3 \text{ (60\%)}.$$

In the downward pass,  $|B_L| \neq |B_R|$ , but in terms of the computational cost estimate, we can assume that they are both  $s/2$ .



The second method is based on (17b), the sequential inverse of the block matrix. Similar to the first method, it does not compute  $\mathbf{A}(\mathbf{S}, \mathbf{S})^{-1}$  explicitly. Instead, it computes  $\mathbf{A}(\mathbf{S}, \mathbf{S})^{-1}\mathbf{A}(\mathbf{S}, \mathbf{B})$  as

$$\begin{pmatrix} A & B \\ C & D \end{pmatrix}^{-1} \begin{pmatrix} W & 0 \\ 0 & Z \end{pmatrix} = \begin{pmatrix} A^{-1}W + A^{-1}B\tilde{D}^{-1}CA^{-1}W & -A^{-1}B\tilde{D}^{-1}Z \\ -\tilde{D}^{-1}CA^{-1}W & \tilde{D}^{-1}Z \end{pmatrix}, \quad (24)$$

where  $\tilde{D} = D - CA^{-1}B$ ,  $B$  and  $C$  are diagonal, and  $X = Y = 0$ . Table 4 shows the required operations with the total cost  $\frac{4}{3}m^3 + 5m^2n + 4mn^2$ .

Table 4: Operation costs in flops and their dependence in the sequential inverse method.

Operation	Cost	Dependency
① $A^{-1}$	$m^3$	n/a
② $\tilde{D}$	0	①
③ $\tilde{D}^{-1}Z$	$\frac{m^3}{3} + m^2n$	②
④ $-(A^{-1}B)(\tilde{D}^{-1}Z)$	$m^2n$	①③
⑤ $A^{-1}W$	$m^2n$	①
⑥ $-\tilde{D}^{-1}(CA^{-1}W)$	$m^2n$	③⑤
⑦ $(A^{-1}W) + (A^{-1}B)(\tilde{D}^{-1}CA^{-1}W)$	$m^2n$	①⑤⑥
⑧ $\mathbf{A}(\mathbf{S}, \mathbf{B})\mathbf{A}(\mathbf{S}, \mathbf{S})^{-1}\mathbf{A}(\mathbf{S}, \mathbf{B})$	$4mn^2$	⑦
<b>Total</b>	$\frac{4}{3}m^3 + 5m^2n + 4mn^2$	n/a

Compared to the previous method, the cost here is smaller if  $m > \frac{3}{4}n$ . Therefore, this method is better than the first method for the downward pass where typically  $(m, n)$  is  $(3a, 2a)$  and  $(4a, 2a)$ . In such cases, the costs are  $174a^3$  (56%) and  $\frac{1408}{3}a^3$  (56%), respectively.

The third method is based on (17c), the block inverse of the block matrix. The two factors there will multiply  $\mathbf{A}(\mathbf{B}, \mathbf{S})$  and  $\mathbf{A}(\mathbf{S}, \mathbf{B})$  separately:

$$\begin{aligned} & \mathbf{A}(\mathbf{B}, \mathbf{S}) \mathbf{A}(\mathbf{S}, \mathbf{S})^{-1} \mathbf{A}(\mathbf{S}, \mathbf{B}) \\ &= \begin{bmatrix} P & 0 \\ 0 & S \end{bmatrix} \begin{bmatrix} A & B \\ 0 & \tilde{D} \end{bmatrix}^{-1} \begin{bmatrix} I & 0 \\ CA^{-1} & I \end{bmatrix}^{-1} \begin{bmatrix} W & 0 \\ 0 & Z \end{bmatrix} \\ &= \begin{bmatrix} P & 0 \\ 0 & S \end{bmatrix} \begin{bmatrix} A^{-1} & -A^{-1}B\tilde{D}^{-1} \\ 0 & \tilde{D}^{-1} \end{bmatrix} \begin{bmatrix} I & 0 \\ -CA^{-1} & I \end{bmatrix} \begin{bmatrix} W & 0 \\ 0 & Z \end{bmatrix} \\ &= \begin{bmatrix} PA^{-1} & -PA^{-1}B\tilde{D}^{-1} \\ 0 & S\tilde{D}^{-1} \end{bmatrix} \begin{bmatrix} W & 0 \\ -CA^{-1}W & Z \end{bmatrix} \end{aligned} \quad (25)$$

The cost of (25) is  $\frac{4}{3}m^3 + 4m^2n + 5mn^2$ , which comes from the multiplication of a block upper triangular matrix and a block lower triangular matrix. Table 5 shows the order and details of the operations.  $S\tilde{D}^{-1}$  is computed by first LU factorizing  $\tilde{D}$  and then solving for  $S\tilde{D}^{-1}$ . The LU form of  $\tilde{D}$  will be used when computing  $-(PA^{-1}B)\tilde{D}^{-1}$  as well.

Finally, our fourth method is more straightforward. We call it *naïve LU method*. It considers  $\mathbf{A}(\mathbf{B}, \mathbf{S})$  and  $\mathbf{A}(\mathbf{S}, \mathbf{B})$  as block diagonal matrices but considers  $\mathbf{A}(\mathbf{S}, \mathbf{S})$  as a full matrix without exploiting its sparsity. This method gives cost  $\frac{8}{3}m^3 + \frac{13}{2}m^2n + 4mn^2$ . Table 6 shows the order and details of the operations. The cost for computing the second column of  $L^{-1}\mathbf{A}(\mathbf{S}, \mathbf{B})$  is reduced since  $\mathbf{A}(\mathbf{S}, \mathbf{B})$  is block diagonal.

The summary of all the optimization techniques for sparsity and the corresponding costs is given in the main body of this paper, in Table 1.

Table 5: Operation costs in flops and their dependence in the block LU inverse method.

	<i>Operation</i>	<i>Cost</i>	<i>Dependency</i>
①	$A^{-1}$	$m^3$	n/a
②	$\tilde{D}$	0	①
③	$\tilde{D}^{-1}Z$	$\frac{m^3}{3} + m^2n$	②
④	$-(A^{-1}B)(\tilde{D}^{-1}Z)$	$m^2n$	①③
⑤	$A^{-1}W$	$m^2n$	①
⑥	$-\tilde{D}^{-1}(CA^{-1}W)$	$m^2n$	③⑤
⑦	$(A^{-1}W) + (A^{-1}B)(\tilde{D}^{-1}CA^{-1}W)$	$m^2n$	①⑤⑥
⑧	$\mathbf{A}(\mathbf{S}, \mathbf{B})\mathbf{A}(\mathbf{S}, \mathbf{S})^{-1}\mathbf{A}(\mathbf{S}, \mathbf{B})$	$4mn^2$	⑦
	<b>Total</b>	$\frac{4}{3}m^3 + 5m^2n + 4mn^2$	n/a

Table 6: Operation cost in flops and their dependence in the naïve LU inverse method.

<i>Operation</i>	<i>Cost</i>
LU for $\mathbf{A}(\mathbf{S}, \mathbf{S})$	$\frac{8}{3}m^3$
$L^{-1}\mathbf{A}(\mathbf{S}, \mathbf{B})$ : 1st block column	$2m^2n$
$L^{-1}\mathbf{A}(\mathbf{S}, \mathbf{B})$ : 2nd block column	$\frac{1}{2}m^2n$
$U^{-1}[L^{-1}\mathbf{A}(\mathbf{S}, \mathbf{B})]$	$4m^2n$
$\mathbf{A}(\mathbf{S}, \mathbf{B})\mathbf{A}(\mathbf{S}, \mathbf{S})^{-1}\mathbf{A}(\mathbf{S}, \mathbf{B})$	$4mn^2$
<b>Total</b>	$\frac{8}{3}m^3 + \frac{13}{2}m^2n + 4mn^2$

Finally, Table 7 shows the estimated level-by-level costs with the physical boundary of the device taken into consideration (see Section “Nodes on the physical boundary of the device”). This cost does not assume any optimization. It simply accounts for the effect of the boundary of the physical device, which leads to a computational cost reduction.

The last two rows for each pass are the sum of the cost of the rest of the small clusters. This estimate does not consider the two end blocks corresponding to the device contacts as in real applications [5, 21]. Accounting for the two end blocks, if we do not have any optimization, then the grand total is:  $450N^3 + \frac{16}{3}N^3 + 2N^3 \approx 457N^3$ . As a comparison, the cost using RGF with symmetry taken into consideration is  $3.5N^4$ . Since the cross-point of the two cost curves is at  $N$  equal to the ratio between the constant factors in the two methods, it is expected to happen at  $N \sim 130$ . This is consistent with the results from our early simulations (between  $N = 100$  and  $N = 150$ ) [5].

*Summary.* The optimization for sparsity leads to 40% cost reduction and that for symmetry leads to 50% cost reduction. This results in a 70% cost reduction. In other words, the new cost is about 1/3 of the original cost. This is reflected in the cross-point of the performance curves using these two methods. Originally, the cross-point was around  $N \sim 130$ , but now it can be as low as  $N = 40$ . This shows the performance improvement resulting from our optimizations. The optimization for sparsity does not reduce the memory cost. The optimization for symmetry does reduce it (approximately by half).

## D Additional proofs

In this section, we present some additional technical results and proofs required to show correctness of our algorithm. All the relevant properties of the mesh node subsets for our algorithm are listed, along with their

Table 7: Computation cost estimate for different type of clusters from an  $N \times N$  mesh.  $s$  is the size of the private inner node set and  $b$  is the size of the boundary set. The size is in unit of  $N$  and the cost is in unit of  $N^3$ . By convention, the root (the whole mesh) of the cluster tree is level 0. The cost column gives the total cost for the given subset of clusters. For example, on row one, under upward pass, we have 2 clusters at level 1 with  $s = 1 N$  and  $b = 1 N$  and the cost for operating on these clusters is  $4.666 N^3$ .

<i>upward pass</i>					<i>downward pass</i>				
<i>size per cluster &amp; total cost</i>			<i>clusters</i>		<i>size &amp; cost per cluster</i>			<i>clusters</i>	
<i>s</i>	<i>b</i>	<i>cost</i>	<i>level</i>	<i>number</i>	<i>s</i>	<i>b</i>	<i>cost</i>	<i>level</i>	<i>number</i>
1	1	4.666	1	2	0	1	0	1	2
1	1	9.332	2	4	1	1	9.332	2	4
1/2	3/4	2.040	3	4	3/2	3/4	14.624	3	4
1/2	5/4	4.540	3	4	1/2	5/4	4.540	3	4
1/2	1	3.168	4	4	1	1/2	4.332	4	4
1/2	3/4	4.080	4	8	1/2	3/4	2.040	4	4
1/2	1/2	1.168	4	4	3/2	3/4	14.624	4	4
1/4	3/8	0.2552	5	4	1	1	9.332	4	4
1/4	1/2	0.3958	5	4	1	3/4	52.672	5	32
1/4	5/8	1.703	5	12	3/4	1/2	38.976	6	64
1/4	3/4	2.312	5	12			<91.648	7...	
1/4	1/2	6.336	6	64					
1/8	3/8	3.072	7	128					
		<9.408	8...						
<b>Subtotal</b>		52.470			<b>Subtotal</b>		242.120		
<b>Total:</b>		<b>294.6</b>							

proofs for the basic FIND algorithm in Li et al. [5]. We will then use these properties to prove two theorems and four corollaries used for computing  $\mathbf{G}^<$ . Some of the properties are not directly used in the proofs but are still listed to help understand the algorithm.

Property 3 is fairly simple but will be used again and again in proving theorems, corollaries, and other properties.

**Property 3** *By definition of  $T_r^+$ , one of the following relations must hold:  $C_i \subset C_j$ ,  $C_i \supset C_j$ , or  $C_i \cap C_j = \emptyset$ .*

Property 4 shows an alternative way of looking at the inner mesh nodes. It helps understand Property 5.

**Property 4**  $l_i = \cup_{C_j \subseteq C_i} S_j$ , where  $C_i$  and  $C_j \in T_r^+$ .

**Property 5** *If  $C_i$  and  $C_j$  are the two children of  $C_k$ , then  $S_k \cup B_k = B_i \cup B_j$  and  $S_k = (B_i \cup B_j) \setminus B_k$ .*

**Property 6** *For any given augmented tree  $T_r^+$  and all  $C_i \in T_r^+$ ,  $S_i$ ,  $B_{-r}$ , and  $C_r$  are all disjoint and  $M = (\cup_{C_i \in T_r^+} S_i) \cup B_{-r} \cup C_r$ .*

Property 6 shows that the whole mesh can be partitioned into subsets  $S_i$ ,  $B_{-r}$ , and  $C_r$ . See Sections “Brief description of the FIND algorithm” and “Formal description of the FIND algorithm” for notations and figures.

Below we list properties of  $S_i$  for specific orderings.

**Property 7** *If  $S_i < S_j$ , then  $C_j \not\subseteq C_i$ , which implies either  $C_i \subset C_j$  or  $C_i \cap C_j = \emptyset$ .*

This property is straightforward from the definition of  $S_i < S_j$  and Property 3.

Properties 8 and 9 below are related to the elimination process. They were used in the proof of the following theorem (see main body of paper, theorem 1):

**Theorem 2** For any target clusters  $r$  and  $s$  such that  $C_g \in \mathbb{T}_r^+$  and  $C_g \in \mathbb{T}_s^+$ , we have

$$\mathbf{A}_{r,g+}(\mathbf{B}_g, \mathbf{B}_g) = \mathbf{A}_{s,g+}(\mathbf{B}_g, \mathbf{B}_g).$$

They will also be used in the proof of Theorem 3 and Theorem 4.

**Property 8** For any  $k, u$  such that  $C_k, C_u \in \mathbb{T}_r^+$ , if  $C_u \not\subseteq C_k$ , then  $\mathbf{B}_u \cap \mathbf{l}_k = \emptyset$ .

*Proof:* By Property 3, we have  $C_u \not\subseteq C_k$ . So for all  $j$  such that  $C_j \subseteq C_k$ , we have  $j \neq u$  and thus  $S_j \cap S_u = \emptyset$  by property 3. By property 2,  $\mathbf{l}_k = \cup_{C_j \subseteq C_k} S_j$ , so we have  $\mathbf{l}_k \cap S_u = \emptyset$ .  $\square$

**Property 9** If  $C_j$  is a child of  $C_k$ , then for any  $C_u$  such that  $S_j < S_u < S_k$ , we have  $C_j \cap C_u = \emptyset$  and thus  $\mathbf{B}_j \cap \mathbf{B}_u = \emptyset$ .

This is because the  $C_u$  can be neither a descendant of  $C_j$  nor an ancestor of  $C_k$ .

In Theorem 3 and its proof below, we follow the same notation used in Li et al. [5]. In particular, we write  $S_g$  more formally as  $S_{i_j}$ , with  $j = 1, 2, \dots$ , etc., where  $\mathbf{A}_{i_1} = \mathbf{A}$ ,  $\Sigma_{i_1} = \Sigma$ , and  $S_{i_j} < S_{i_{j'}}$  iff  $j < j'$ . We also denote  $S_{i_{j+1}}$  as  $S_{g+}$  when  $g = i_j$ . Because of Property 6, the whole mesh  $\mathbf{M}$  is partitioned into a sequence of sets  $S_{i_j}$ ,  $\mathbf{B}_{-r}$ , and  $\mathbf{C}_r$ ,  $j = 1, 2, \dots$ , and the order of  $\mathbf{A}$  and  $\Sigma$  is determined by this sequence. For notation convenience, if  $i$  is the index of the last set in the sequence of  $S_{i_j}$ , which is always  $-r$  for  $\mathbb{T}_r^+$ , then  $S_{i+}$  stands for  $\mathbf{B}_{-r}$ .

**Theorem 3** If we perform Gaussian elimination as described in the Section ‘‘Formal description of the FIND algorithm’’ and update  $\Sigma_g$  accordingly based on  $\Sigma_{g+} = \mathbf{L}_g^{-1} \Sigma_g \mathbf{L}_g^{-\dagger}$ , then we have:

$$(I) \quad \forall S_h \geq S_g, \Sigma_g(S_h, S_{>h} \setminus \mathbf{B}_h) = \Sigma_g(S_{>h} \setminus \mathbf{B}_h, S_h) = 0;$$

$$(II) \quad (a) \quad \Sigma_{g+}(S_{\leq g}, S_{\leq g}) = \Sigma_g(S_{\leq g}, S_{\leq g});$$

$$(b) \quad \Sigma_{g+}(\mathbf{M}, S_{>g} \setminus \mathbf{B}_g) = \Sigma_g(\mathbf{M}, S_{>g} \setminus \mathbf{B}_g);$$

$$(c) \quad \Sigma_{g+}(S_{>g} \setminus \mathbf{B}_g, \mathbf{M}) = \Sigma_g(S_{>g} \setminus \mathbf{B}_g, \mathbf{M});$$

$$(III) \quad \Sigma_{g+}(\mathbf{B}_g, \mathbf{B}_g) = \Sigma_g(\mathbf{B}_g, \mathbf{B}_g) - \mathcal{L}_g \Sigma_g(S_g, \mathbf{B}_g) - \Sigma_g(\mathbf{B}_g, S_g) \mathcal{L}_g^\dagger + \mathcal{L}_g \Sigma_g(S_g, S_g) \mathcal{L}_g^\dagger.$$

In other word, this theorem describes how the multiplications by  $\mathbf{L}_g^{-1}$  and  $\mathbf{L}_g^{-\dagger}$  affect  $\Sigma_g$ . Specifically, these multiplications only affect  $\Sigma_g(\mathbf{B}_g, \mathbf{B}_g)$ , which is given by (III), and  $\Sigma_g(S_{\leq g}, \mathbf{B}_g)$  and  $\Sigma_g(\mathbf{B}_g, S_{\leq g})$ , which are not given here but can be ignored. The multiplication preserves the sparsity pattern specified by (I) above, which is illustrated by the following submatrix for any  $S_h > S_g$ :<sup>9</sup>

$$\begin{array}{ccc} & S_h & \mathbf{B}_h & S_{>h} \setminus \mathbf{B}_h \\ S_h & \times & \times & \mathbf{0} \\ \mathbf{B}_h & \times & \times & \times \\ S_{>h} \setminus \mathbf{B}_h & \mathbf{0} & \times & \times \end{array}$$

*Proof:* Recall that  $-\mathcal{L}_g = -\mathbf{L}_g(\mathbf{B}_g, S_g)$  is the only non-zero off-diagonal block of  $\mathbf{L}_g^{-1}$ . As a result, all entries in  $\Sigma_g(\bullet, S_{<g})$  and  $\Sigma_g(S_{<g}, \bullet)$  are irrelevant to the multiplication and (I) implies (II) and (III). So it suffices to prove (I) by mathematical induction.

For  $g = i_1$ , (I) holds because no nodes in  $S_h$  and  $S_{>h} \setminus \mathbf{B}_h$  are connected to each other and in the original matrix  $\Sigma$ , an entry is non-zero iff the two nodes associated with the column and the array of the entry connect to each other. If (I) holds for  $g = k$ , then by Property 3 we have either  $C_k \subset C_{k+}$  or  $C_k \cap C_{k+} = \emptyset$ . So,

<sup>9</sup>Similar to the notation  $\mathbf{A}_g(\bullet, \mathbf{B}_g)$ , the entries of the blocks in this submatrix usually do *not* stay together (except the entries of  $\Sigma_g(S_h, S_h)$ , which always stay together). We write them here like blocks to better illustrate the sparsity pattern of  $\Sigma_g$ .

- if  $C_k \subset C_{k+}$ , consider  $u$  such that  $S_{k+} < S_u$ . By Property 8, we have  $I_{k+} \cap S_u = \emptyset$ . Since  $C_{k+} = I_{k+} \cup B_{k+}$ , we have  $(S_u \setminus B_{k+}) \cap C_{k+} = \emptyset$ . So we have  $B_k \cap (S_u \setminus B_{k+}) \subseteq (S_u \setminus B_{k+}) \cap C_k \subseteq (S_u \setminus B_{k+}) \cap C_{k+} = \emptyset \Rightarrow B_k \cap (S_{>k+} \setminus B_{k+}) = \emptyset$ ;
- if  $C_k \cap C_{k+} = \emptyset$ , then  $B_k \subset C_k$  and  $S_{k+} \subset C_{k+} \Rightarrow B_k \cap S_{k+} = \emptyset$ .

So in both cases, we have  $(B_k, B_k) \cap (S_{k+}, S_{>k+} \setminus B_{k+}) = \emptyset$ . In addition, by Property 6, we have  $S_k \cap S_{k+} = \emptyset$ . Since all (I), (II), and (III) hold for  $g = k$ , we have  $\Sigma_{k+}(S_{k+}, S_{>k+} \setminus B_{k+}) = \Sigma_{k+}(S_{>k+} \setminus B_{k+}, S_{k+}) = \mathbf{0}$ .

Since the above argument is valid for all  $h \geq k+$ , we have  $\forall h \geq k+$ ,  $\Sigma_{k+}(S_h, S_{>h} \setminus B_h) = \Sigma_{k+}(S_{>h} \setminus B_h, S_h) = \mathbf{0}$ , i.e., (I) holds for  $g = k+$  as well. By induction, we have that (I) holds for all  $g$  such that  $C_g \in \mathbb{T}_r^+$ .  $\square$

**Corollary 1** *If  $C_i$  and  $C_j$  are the two children of  $C_k$ , then  $\Sigma_k(B_i, B_j) = \Sigma(B_i, B_j)$  and  $\Sigma_k(B_j, B_i) = \Sigma(B_j, B_i)$ .*

In words, the corollary states that when we compute  $\mathbf{L}_k^{-1} \Sigma_k \mathbf{L}_k^{-\dagger}$ , we can take some of the entries in  $\Sigma_k$  directly from the original  $\Sigma$ .

**Proof:** By Theorem 3, the multiplications by  $\mathbf{L}_u^{-1}$  and  $\mathbf{L}_u^{-\dagger}$  only change the entries of  $\Sigma_u$  in  $(B_u, B_u)$ ,  $(S_{\leq u}, B_u)$ , and  $(B_u, S_{\leq u})$ . So it suffices to show that for every  $S_u < S_k$ , we have

$$(B_u, B_u) \cap (B_i, B_j) = \emptyset, \quad (26)$$

$$(S_{\leq u}, B_u) \cap (B_i, B_j) = (B_u, S_{\leq u}) \cap (B_i, B_j) = \emptyset, \quad (27)$$

and similar identities with  $i$  and  $j$  interchanged.

To show (26), consider the following three cases:

- $C_u \cap C_k = \emptyset \Rightarrow C_u \cap C_i = C_u \cap C_j = \emptyset \Rightarrow B_u \cap B_i = B_u \cap B_j = \emptyset$ ;
- $C_u \subset C_i \Rightarrow C_u \cap C_j = \emptyset \Rightarrow B_u \cap B_j = \emptyset$ ;
- $C_u \subset C_j \Rightarrow C_u \cap C_i = \emptyset \Rightarrow B_u \cap B_i = \emptyset$ .

Because  $\forall S_u < S_k$ , by Property 7 (with some extension), one of the above cases must hold. So we have proved (26).

To show (27), consider  $S_v < S_k$ . Because

$$S_v < S_k \Rightarrow C_k \not\subset C_v \Rightarrow C_i \not\subset C_v$$

by Property 7, we have either

$$C_v \cap C_i = \emptyset \Rightarrow S_v \cap B_i = \emptyset$$

or

$$C_v \subset C_i \text{ (by Property 4)} \Rightarrow S_v \subset I_i \Rightarrow S_v \cap B_i = \emptyset.$$

We can also conclude  $S_v \cap B_j = \emptyset$  by a similar argument, so we have proved (27).  $\square$

**Corollary 2** *If  $C_i$  is a child of  $C_k$ , then  $\Sigma_k(B_i, B_i) = \Sigma_{i+}(B_i, B_i)$ .*

**Proof:** Consider  $u$  such that  $S_i < S_u < S_k$ . By Property 9, we have  $B_i \cap B_u = \emptyset$ . By Theorem 3, the multiplications by  $\mathbf{L}_u^{-1}$  and  $\mathbf{L}_u^{-\dagger}$  only change the entries of  $\Sigma_u$  in  $(B_u, B_u)$ ,  $(S_{\leq u}, B_u)$ , and  $(B_u, S_{\leq u})$  and none of them will change the entries in  $(B_i, B_i)$ , so the corollary is proved.  $\square$

**Corollary 3** *If  $C_i$  is a leaf node in  $\mathbb{T}_r^+$ , then  $\Sigma_i(C_i, C_i) = \Sigma(C_i, C_i)$ .*

**Proof:** Consider  $S_u < S_i$ . By Property 3, either  $C_u \subset C_i$  or  $C_u \cap C_i = \emptyset$ . Since  $C_i$  is a leaf node, there is no  $u$  such that  $C_u \subset C_i$ . So we have  $C_u \cap C_i = \emptyset$  and thus  $B_u \cap C_i = \emptyset$ . By theorem 3, the corollary is proved.  $\square$

**Theorem 4** *For any  $r$  and  $s$  such that  $C_i \in \mathbb{T}_r^+$  and  $C_i \in \mathbb{T}_s^+$ , we have:*

$$\Sigma_{r,i}(S_i \cup B_i, S_i \cup B_i) = \Sigma_{s,i}(S_i \cup B_i, S_i \cup B_i) \quad (28)$$

**Proof:** If  $C_i$  is a leaf node, then by Corollary 3, we have  $\Sigma_{r,i}(S_i \cup B_i, S_i \cup B_i) = \Sigma_{r,i}(C_i, C_i) = \Sigma_r(C_i, C_i) = \Sigma_s(C_i, C_i) = \Sigma_{s,i}(C_i, C_i) = \Sigma_{s,i}(S_i \cup B_i, S_i \cup B_i)$

If (28) holds for  $i$  and  $j$  such that  $C_i$  and  $C_j$  are the two children of  $C_k$ , then

- by Theorem 3, we have
  - ◊  $\Sigma_{r,i+}(B_i, B_i) = \Sigma_{s,i+}(B_i, B_i)$  and
  - ◊  $\Sigma_{r,j+}(B_j, B_j) = \Sigma_{s,j+}(B_j, B_j)$ ;
- by Corollary 1, we have
  - ◊  $\Sigma_{r,k}(B_i, B_j) = \Sigma_r(B_i, B_j) = \Sigma_s(B_i, B_j) = \Sigma_{s,k}(B_i, B_j)$  and
  - ◊  $\Sigma_{r,k}(B_j, B_i) = \Sigma_r(B_j, B_i) = \Sigma_s(B_j, B_i) = \Sigma_{s,k}(B_j, B_i)$ .
- by Corollary 2, we have
  - ◊  $\Sigma_{r,k}(B_i, B_i) = \Sigma_{r,i+}(B_i, B_i) = \Sigma_{s,i+}(B_i, B_i) = \Sigma_{s,k}(B_i, B_i)$  and
  - ◊  $\Sigma_{r,k}(B_j, B_j) = \Sigma_{r,j+}(B_j, B_j) = \Sigma_{s,j+}(B_j, B_j) = \Sigma_{s,k}(B_j, B_j)$ ;

Now we have  $\Sigma_{r,k}(B_i \cup B_j, B_i \cup B_j) = \Sigma_{s,k}(B_i \cup B_j, B_i \cup B_j)$ . By Property 5, we have  $\Sigma_{r,k}(S_k \cup B_k, S_k \cup B_k) = \Sigma_{s,k}(S_k \cup B_k, S_k \cup B_k)$ . By induction, the theorem is proved.  $\square$

**Corollary 4** For any  $r$  and  $s$  such that  $C_i \in \mathbb{T}_r^+$  and  $C_i \in \mathbb{T}_s^+$ , we have:

$$\Sigma_{r,i+}(B_i, B_i) = \Sigma_{s,i+}(B_i, B_i)$$

This corollary shows that the update processes for two target clusters  $C_r$  and  $C_s$  share their partial results so we can reuse them in our algorithm. The proof is trivial given Theorem 3 and Theorem 4.

## References

- [1] S. Datta, Electronic Transport in Mesoscopic Systems, Cambridge University Press, 1997. 3
- [2] A. Svizhenko, M. P. Anantram, T. Govindan, B. Biegel, R. Venugopal, Two-dimensional quantum mechanical modeling of nanotransistors, Journal of Applied Physics 91 (4) (2002) 2343–2354. 3
- [3] A. Ghosh, P. Damle, S. Datta, A. Nitzan, Molecular Electronics, Materials Research Society bulletin (2004) 391. 3
- [4] A. Martinez, M. Bescond, J. Barker, A. Svizhenko, M. Anantram, C. Millar, A. Asenov, A self-consistent full 3-D real-space NEGF simulator for studying nonperturbative effects in nano-MOSFETs, IEEE Transactions on Electron Devices 54 (9) (2007) 2213–2222. 3
- [5] S. Li, S. Ahmed, G. Klimeck, E. Darve, Computing entries of the inverse of a sparse matrix using the FIND algorithm, Journal of Computational Physics 227 (2008) 9408–9427. 3, 4, 7, 8, 10, 13, 21, 26, 27, 28
- [6] E. Darve, S. Li, Y. Teslyar, Calculating transport properties of nanodevices, in: Proceedings of SPIE, Philadelphia, PA, Vol. 5593, 2004, pp. 452–463. 3, 4
- [7] S. Li, S. Ahmed, E. Darve, Fast inverse using nested dissection for NEGF, Journal of Computational Electronics 6 (2007) 187–190. 3, 4
- [8] R. Lake, G. Klimeck, R. Bowen, D. Jovanovic, Single and multiband modeling of quantum electron transport through layered semiconductor devices, Journal of Applied Physics 81 (1997) 7845. 3
- [9] S. Börm, L. Grasedyck, W. Hackbusch, Hierarchical matrices, Lecture note, Citeseer 21 (2003) 1–124. 3, 4
- [10] W. Hackbusch, A sparse matrix arithmetic based on  $\mathcal{H}$ -matrices. Part I: Introduction to  $\mathcal{H}$ -matrices, Computing 62 (2) (1999) 89–108. 3

- [11] S. Chandrasekaran, P. Dewilde, M. Gu, T. Pals, X. Sun, A. van der Veen, D. White, Some fast algorithms for sequentially semiseparable representations, *Siam Journal on Matrix Analysis and Applications* 27 (2) (2006) 341–364. 4
- [12] S. Chandrasekaran, M. Gu, T. Pals, A fast ULV decomposition solver for hierarchically semiseparable representations, *SIAM Journal on Matrix Analysis and Applications* 28 (2006) 603–622. 4
- [13] S. Chandrasekaran, P. Dewilde, M. Gu, W. Lyons, T. Pals, A fast solver for HSS representations via sparse matrices, *Siam Journal on Matrix Analysis and Applications* 29 (1) (2008) 67–81. 4
- [14] D. Mamaluy, M. Sabathil, P. Vogl, Efficient method for the calculation of ballistic quantum transport, *Journal of Applied Physics* 93 (8) (2003) 4628–33. 4
- [15] H. Khan, D. Mamaluy, D. Vasileska, Quantum transport simulation of experimentally fabricated nano-FinFET, *IEEE Transactions on Electron Devices* 54 (4) (2007) 784. 4
- [16] M. Sabathil, D. Mamaluy, P. Vogl, Prediction of a realistic quantum logic gate using the contact block reduction method, *Semiconductor Science and Technology* 19 (2004) S137–S138. 4
- [17] D. Mamaluy, A. Mannargudi, D. Vasileska, M. Sabathil, P. Vogl, Contact block reduction method and its application to a 10 nm MOSFET device, *Semiconductor Science and Technology* 19 (2004) S118–S121. 4
- [18] D. Mamaluy, A. Mannargudi, D. Vasileska, Electron Density Calculation Using the Contact Block Reduction Method, *Journal of Computational Electronics* 3 (1) (2004) 45–50. 4
- [19] S. Birner, C. Schindler, P. Greck, M. Sabathil, P. Vogl, Ballistic quantum transport using the contact block reduction (CBR) method, *Journal of Computational Electronics* 8 (3) (2009) 267–286. 4
- [20] J. Tang, Y. Saad, A probing method for computing the diagonal of the matrix inverse, Tech. rep., Tech. Report umsi-2010-42, Minnesota Supercomputer Institute, University of Minnesota, Minneapolis, MN, 2009 (2010). 4
- [21] A. Svizhenko, M. P. Anantram, T. R. Govindan, B. Biegel, Two-dimensional quantum mechanical modeling of nanotransistors, *Journal of Applied Physics* 91 (4) (2002) 2343–54. 4, 8, 13, 16, 26
- [22] A. Erisman, W. Tinney, On computing certain elements of the inverse of a sparse matrix, *Communications of the ACM* 18 (3) (1975) 177–179. 4
- [23] D. Petersen, H. Sørensen, P. Hansen, S. Skelboe, K. Stokbro, Block tridiagonal matrix inversion and fast transmission calculations, *J. Comput. Phys.* 227 (2008) 3174–3190. 4
- [24] L. Lin, J. Lu, L. Ying, R. Car, Fast algorithm for extracting the diagonal of the inverse matrix with application to the electronic structure analysis of metallic systems, *Communications in Mathematical Sciences* 7 (3) (2009) 755–777. 4
- [25] L. Lin, C. Yang, J. Meza, J. Lu, L. Ying, SelInv—An Algorithm for Selected Inversion of a Sparse Symmetric Matrix, *ACM Transactions on Mathematical Software (TOMS)* 37 (4) (2011) 40. 4
- [26] A. George, Nested dissection of a regular finite-element mesh, *SIAM Journal on Numerical Analysis* 10 (2) (1973) 345–63. 4, 8
- [27] J. Liu, The solution of mesh equations on a parallel computer, Dep. of Computer Science, Univ., 1974. 4
- [28] A. George, E. Ng, On row and column orderings for sparse least squares problems, *SIAM Journal on Numerical Analysis* 20 (2) (1983) 326–344. 4

- [29] J. Gilbert, E. Zmijewski, A parallel graph partitioning algorithm for a message-passing multiprocessor, *International Journal of Parallel Programming* 16 (6) (1987) 427–449. 4
- [30] A. Pothen, H. Simon, K. Liou, Partitioning sparse matrices with eigenvectors of graphs, *SIAM Journal on Matrix Analysis and Applications* 11 (3). 4
- [31] M. Heath, E. Ng, B. Peyton, Parallel algorithms for sparse linear systems, *SIAM review* 33 (3) (1991) 420–460. 4
- [32] D. Petersen, S. Li, K. Stokbro, H. Sørensen, P. Hansen, S. Skelboe, E. Darve, A hybrid method for the parallel computation of Green’s functions, *Journal of Computational Physics* 228 (14) (2009) 5020–5039. 8
- [33] G. H. Golub, C. F. Van Loan, *Matrix Computations*, Third Edition, Johns Hopkins University Press, 1996. 16, 22
- [34] J. R. Bunch, B. N. Parlett, Direct methods for solving symmetric indefinite systems of linear equations, *SIAM Journal on Numerical Analysis* 8 (1971) 639–55. 16
- [35] J. R. Bunch, L. Kaufman, Some stable methods for calculating inertia and solving symmetric linear systems, *Mathematics of Computation* 31 (1977) 162–79. 16
- [36] U. Trottenberg, T. Clees, Multigrid software for industrial applications — from MG00 to SAMG, *100 Volumes of Notes on Numerical Fluid Mechanics* (2009) 423–436. 21
- [37] A. Brandt, General highly accurate algebraic coarsening, *Electronic Transactions on Numerical Analysis* 10 (1). 21
- [38] J. Fattebert, J. Bernholc, Towards grid-based  $O(N)$  density-functional theory methods: Optimized nonorthogonal orbitals and multigrid acceleration, *Physical Review B* 62 (3) (2000) 1713. 21
- [39] J. Bernholc, M. Hodak, W. Lu, Recent developments and applications of the real-space multigrid method, *Journal of Physics: Condensed Matter* 20 (2008) 294205. 21
- [40] G. Feng, T. Beck, Nonlinear multigrid eigenvalue solver utilizing nonorthogonal localized orbitals, *Physica Status Solidi (b)* 243 (5) (2006) 1054–1062. 21
- [41] N. Wijesekera, G. Feng, T. Beck, Efficient multiscale algorithms for solution of self-consistent eigenvalue problems in real space, *Physical Review B* 75 (11) (2007) 115101. 21